MULTI-COLOR OPTICAL AND NEAR-INFRARED LIGHT CURVES OF 64 STRIPPED-ENVELOPE CORE-COLLAPSE SUPERNOVAE

The Astrophysical Journal Supplement Series, 213:19 (21pp), 2014 August doi:10.1088/0067-0049/213/2/19

MULTI-COLOR OPTICAL AND NEAR-INFRARED LIGHT CURVES OF 64 STRIPPED-ENVELOPE CORE–COLLAPSE SUPERNOVAE

F. B. Bianco[1], M. Modjaz[1], M. Hicken[2], A. Friedman[2,3], R. P. Kirshner[2],
J. S. Bloom[4,5], P. Challis[2], G. H. Marion[2,6], W. M. Wood-Vasey[7], and A. Rest[8]
[1] Center for Cosmology and Particle Physics, New York University, 4 Washington Place, New York, NY 10003, USA; fb55@nyu.edu
[2] Harvard-Smithsonian Center for Astrophysics, 60 Garden Street, Cambridge, MA 02138, USA
[3] Center for Theoretical Physics and Department of Physics, Massachusetts Institute of Technology, Cambridge, MA 02139, USA
[4] Department of Astronomy, University of California, Berkeley, CA 94720-3411, USA
[5] Physics Division, Lawrence Berkeley National Laboratory, 1 Cyclotron Road, Berkeley, CA 94720, USA
[6] Astronomy Department, University of Texas at Austin, Austin, TX 78712, USA
[7] PITT PACC, Department of Physics and Astronomy, 3941 O'Hara Street, University of Pittsburgh, Pittsburgh, PA 15260, USA
[8] Space Telescope Science Institute, 3700 San Martin Drive, Baltimore, MD 21218, USA
Received 2014 March 25; accepted 2014 May 19; published 2014 July 10

ABSTRACT

We present a densely sampled, homogeneous set of light curves of 64 low-redshift ($z \lesssim 0.05$) stripped-envelope supernovae (SNe of Type IIb, Ib, Ic, and Ic-BL). These data were obtained between 2001 and 2009 at the Fred L. Whipple Observatory (FLWO) on Mount Hopkins in Arizona, with the optical FLWO 1.2 m and the near-infrared (NIR) Peters Automated Infrared 1.3 m telescopes. Our data set consists of 4543 optical photometric measurements on 61 SNe, including a combination of *UBVRI*, *UBVr′i′*, and *u′BVr′i′*, and 1919 JHK_s NIR measurements on 25 SNe. This sample constitutes the most extensive *multi-color* data set of stripped-envelope SNe to date. Our photometry is based on template-subtracted images to eliminate any potential host-galaxy light contamination. This work presents these photometric data, compares them with data in the literature, and estimates basic statistical quantities: date of maximum, color, and photometric properties. We identify promising color trends that may permit the identification of stripped-envelope SN subtypes from their photometry alone. Many of these SNe were observed spectroscopically by the Harvard-Smithsonian Center for Astrophysics (CfA) SN group, and the spectra are presented in a companion paper. A thorough exploration that combines the CfA photometry and spectroscopy of stripped-envelope core–collapse SNe will be presented in a follow-up paper.

Key word: supernovae: general

Online-only material: color figures, machine-readable tables

1. INTRODUCTION

Stripped-envelope core–collapse supernovae (stripped SNe) arise from the spectacular deaths of massive stars that have been stripped of their outer layers of hydrogen and helium. In this paper, we present photometric data in optical and near-infrared (NIR) wavelengths for 64 stripped SNe, data that we collected between 2001 and 2009 at the Fred L. Whipple Observatory (FLWO) on Mount Hopkins in Arizona.

Stripped SNe include SNe of types Ib, Ic, and IIb. Type Ib (SNe Ib) and Type Ic SNe (SNe Ic) are SNe that do not show hydrogen lines (thus Type I), but do not exhibit the strong Si II absorption lines characteristic of SNe Ia (Uomoto & Kirshner 1986; Clocchiatti et al. 1997). SNe Ib show conspicuous lines of He I, while SNe Ic do not. SNe IIb change as they age: initially they show strong hydrogen features (hence the Type II classification), but over time, the Balmer series decreases in strength, while the series of He I lines characteristic of SN Ib grows stronger (e.g., Filippenko et al. 1993). Finally, broad-lined SNe Ic (SN Ic-BL) exhibit broad and blended lines in a SNe-Ic-like spectrum, indicative of very high expansion velocities (Galama et al. 1998; Patat et al. 2001; Pian et al. 2006; Modjaz et al. 2006; Sanders et al. 2012). SNe Ic-BL are the only type of SN that have been observed in conjunction with long-duration gamma-ray bursts (GRBs; e.g., Galama et al. 1998; Stanek et al. 2003; Hjorth et al. 2003; Modjaz et al. 2006); see Woosley & Bloom (2006), Modjaz (2011), and Hjorth & Bloom (2012) for reviews of GRB–SN connections. For a review of SN spectroscopic classification, see Filippenko (1997).

Stripped SNe have been studied less than SNe Ia. These SNe, however, are intrinsically almost as common per volume as SNe Ia (Li et al. 2011). They hold vital clues about the death and explosion properties of very massive stars (Uomoto & Kirshner 1986) and their nucleosynthesis products that contribute to the universe's chemical enrichment (Burbidge et al. 1957; Nomoto et al. 2006). The characteristics of the progenitor channels, and their link to each SN class and subclass are not yet well understood nor do we know which is the dominant process responsible for stripping these massive stars of their outer layers: models propose that stripping may occur through strong winds (Woosley et al. 1993) or binary interaction (Nomoto et al. 1995; Podsiadlowski et al. 2004).

Several stripped SNe have been studied in detail individually, beginning with the SN Ic 1994I in the nearby galaxy M 51 (e.g., Richmond et al. 1996; Filippenko et al. 1995). Because of its proximity, it was well observed over many wavelengths and it is commonly referred to as the "prototypical" normal SNe Ic (e.g., Elmhamdi et al. 2006; Sauer et al. 2006).

However, in order to assess the peculiarities of these explosions and to understand the characteristics of stripped SNe, well-observed SNe must be evaluated in the context of a sample large enough to be studied with a statistical approach. For example, SN 1994I appears to be *atypical*: Richardson et al. (2006) and Drout et al. (2011) showed that SN 1994I had a faster light

curve than any other SN Ic in the literature and is a 2σ outlier of the overall distribution of light curves of SNe Ib and SNe Ic.

Richardson et al. (2006) compiled light curves of 27 stripped-envelope SNe from the literature, of which one-third had been found or observed with photographic plates. However, photographic plate surveys are strongly biased against dim SNe or SNe near the nucleus of the host galaxy. Modern CCD surveys, analyzed with image subtraction techniques (Smith et al. 2002), should instead be nearly complete, barring large amounts of host-galaxy dust extinction.

A sample of stripped SNe was presented in Drout et al. (2011; henceforth D11): 25 SNe Ib, Ic, and Ic-BL, observed in two bands. Eighteen of these objects were also observed within our program. D11 concluded that SNe Ib and Ic are indistinguishable photometrically. Furthermore, from the peak luminosity, D11 sets constraints on the ^{56}Ni mass generated in the explosion and, assuming that SNe Ib and SNe Ic have the same photospheric velocities, D11 derives constraints on the ejecta mass from the light curve shape. This pioneering study of stripped SNe, however, presents data in just two bands and does not employ galaxy subtraction. As we show in Section 5, galaxy subtraction can be important for producing accurate light curves.

Li et al. (2011) presented unfiltered light curves of SNe that were discovered as part of the Lick Observatory SN Search (LOSS; Filippenko et al. 2001), including about 30 stripped SNe (5 of which are included in this study). Those unfiltered light curves were crucial for calculating the SN luminosity function and the LOSS SN rates; however, they are in a single, non-standard band.

A collection of UV light curves of core–collapse SNe from *Swift* (Gehrels et al. 2004), including 15 stripped SNe (6 of which are in our sample), is presented in Pritchard et al. (2013). Cano (2013) has recently collected all available *BVRI* photometry of stripped SNe in the literature, a total of 61 objects, and analyzed their bolometric properties, coming to the conclusion that SNe Ib and SNe Ic likely arise from different progenitor channels than SNe Ic-BL.

Understanding the full range of massive star explosion properties requires the study of a large and comprehensive SN sample with homogeneous and densely sampled data. Moreover, the current SN classification scheme, outlined above, is based on spectroscopy. As we enter the era of all-sky optical transient searches, with hundreds, even thousands of SNe to be discovered each night (LSST Science Collaboration & LSST Project 2009), we will simply be unable to obtain systematic spectroscopic follow-up data of most objects. Devising photometric criteria for classifying SNe without spectra is important (Sako et al. 2014). The first step in this process is to obtain well-sampled light curves of SNe Ib, SN Ic, and SN IIb.

This work presents a densely sampled, multi-color, homogeneous data set of stripped SNe, supported and complemented by spectroscopic data (Modjaz et al. 2014, henceforth M14). Since 1993, spectroscopic *and* photometric monitoring of nearby and newly discovered SNe at the FLWO on Mount Hopkins in Arizona has been undertaken by the Harvard-Smithsonian Center for Astrophysics (CfA).[9] Furthermore, the CfA conducted a parallel NIR photometric campaign with Peters Automated Infrared Telescope (PAIRITEL) at FLWO starting in 2004. While, due to their cosmological relevance, SN Ia were prioritized targets throughout the campaign (Riess et al. 1999; Jha et al. 2006; Hicken et al. 2009, 2012), an intense follow-up program of stripped SNe began in 2004, in addition to the SNe Ia follow-up. Here we present photometric data of nearby ($z \lesssim 0.047$) stripped SNe collected between 2001 and 2009. In a second paper (F. B. Bianco et al., in preparation), we will present a deeper analysis of the sample, integrate it with data from the literature, discuss statistical differences in the photometry and colors of different stripped SN subtypes, and derive constraints on their progenitors.

The data set presented in this paper includes 4543 optical photometric observations of 61 SNe (Section 3.1), and 1919 NIR observations of 25 SNe (Section 3.2). All photometry presented here is available in the online version of the journal and at the CfA[10] and New York University[11] supernova group Web sites. The CfA spectroscopic observations of 54 of our SNe are presented in M14.

2. DISCOVERY

The nearby SNe we monitored at the CfA were discovered by a variety of professional SN searches as well as amateurs using modern CCD technology. Systematic SN searches include LOSS, the Texas SN Search (Quimby 2006), The Chilean Automatic Supernova Search (Hamuy et al. 2012), and the Nearby SN Factory (Aldering et al. 2002). SN 2008D was discovered in the X-ray with *Swift* (Soderberg et al. 2008, in X-ray observations of SN 2007uy, an unrelated stripped SN discovered in the same galaxy). The LOSS survey and many amateur SN searches observe in a relatively small field of view (FOV, $8\farcm7 \times 8\farcm7$ for LOSS) and recursively monitor the same galaxies. Typically, these surveys concentrate on well-known luminous galaxies (e.g., Li et al. 2001; Gallagher et al. 2005; Mannucci et al. 2005). Conversely, the Texas SN Search and the Nearby SN Factory are rolling searches with a large FOV (2 and 3 deg^2, respectively) with thousands of galaxies searched impartially.

We list the objects in our SN sample and their basic discovery data in Table 1. Our decision to monitor a particular newly discovered SN Ib, SN Ic, or SN IIb was broadly informed by three considerations: *accessibility* (declination $\gtrsim -20°$), *brightness* ($m < 18$ mag for spectroscopic observations and $m < 20$ mag for optical photometry), and *age* (SNe whose spectra indicated a young age were given higher priority). Of course, the latter two criteria are correlated since older SNe are dimmer.

FLWO undergoes a shut down during the month of August every year due to the Arizona monsoon season. Thus, we have no monitoring data for one month each year.

The 37 SNe in our sample that were studied in the literature prior to this work (and to M14) are noted in Table 1. Twenty-two of these were previously studied *individually* (i.e., not just as part of a survey) in the literature. However, the optical and/or NIR light curves are published for only 18 of these 22 SNe. In some cases (e.g., SN 2007ke, Section 7.2), the only photometric data published are in a single band while our data always provide multi-band coverage in a minimum of three photometric bands. The photometry for an additional 17 stripped SNe that are part of our sample appeared in D11 in the *V* and *R* bands.

The host-galaxy characteristics for all of our objects are listed in Table 2.

[9] http://www.cfa.harvard.edu/oir/Research/supernova/

[10] http://www.cfa.harvard.edu/oir/Research/supernova/

[11] http://www.cosmo.nyu.edu/SNYU

Table 1
Discovery and Classification Data for SN Sample

SN Name	CfA Spectra[a]	CfA NIR[b]	R.A.	Decl.	SN Type[c]	Discovery Date	Discovery Reference	Spectroscopic ID[c]
SN 2001ej	M14		7:23:43	+33:26:38.0	Ib	2001 Sep 17	IAUC 7719	IAUC 7721
SN 2001gd[3]	M14		13:13:23	+36:38:17.7	IIb	2001 Nov 24	IAUC 7761	IAUC 7765
SN 2002ap[1]	M14		1:36:23	+15:45:13.2	Ic-BL	2002 Jan 29	IAUC 7810	IAUC 7811/7825
SN 2003jd[1]	M14		21:03:38	-4:53:45	Ic-BL	2003 Oct 25	IAUC 8232	IAUC 8234
SN 2004ao[1]	M14		17:28:09	+07:24:55.5	Ib	2004 Mar 7	IAUC 8299	IAUC 8430
SN 2004aw[1]	M14		11:57:50	+25:15:55.1	Ic	2004 Mar 19	IAUC 8310	IAUC 8331
SN 2004fe	M14		0:30:11	+02:05:23.5	Ic	2004 Oct 30	IAUC 8425	IAUC 8426
SN 2004gk[1,2]	M13	Y	12:25:33	+12:15:39.9	Ic	2004 Nov 25	IAUC 8446	IAUC 8446
SN 2004gq[2,3]	M14	Y	5:12:04	-15:40:54	Ib	2004 Dec 11	IAUC 8452	IAUC 8452/8461
SN 2004gt[2,4]	M14	Y	12:01:50	-18:52:12	Ic	2004 Dec 12	IAUC 8454	M14
SN 2004gv[2]	M14		2:13:37	-0:43:05.8	Ib	2004 Dec 13	IAUC 8454	IAUC 8456
SN 2005az[2]	M14	Y	13:05:46	+27:44:08.4	Ic	2005 Mar 28	IAUC 8503	IAUC 8504
SN 2005bf[1]	M14	Y	10:23:57	-3:11:28	Ib	2005 Apr 6	IAUC 8507	IAUC 8521
SN 2005ek[1]	M14	Y*	3:05:48	+36:46:10	Ic	2005 Sep 24	IAUC 8604	CBET 235
SN 2005hg[2]	M14	Y	1:55:41	+46:47:47.4	Ib	2005 Oct 25	IAUC 8623	CBET 271
SN 2005kf	M14		7:47:26	+26:55:32.4	Ic	2005 Nov 11	IAUC 8630	CBET 301
SN 2005kl	M14	Y	12:24:35	+39:23:03.5	Ic	2005 Nov 22	CBET 300	CBET 305
SN 2005kz[2]			19:00:49	+50:53:01.8	Ic	2005 Dec 1	IAUC 8639	IAUC 8639
SN 2005la[1,2,d]	M14		12:52:15	+27:31:52.5	Ib-n/IIb-n	2005 Nov 30	IAUC 8639	IAUC 8639
SN 2005mf[2]	M14	Y	9:08:42	+44:48:51.4	Ic	2005 Dec 25	IAUC 8648	IAUC 8650
SN 2005nb[2]	M14		12:13:37	+16:07:16.2	Ic-BL	2005 Dec 17	CBET 357	IAUC 8657
SN 2006F[2]			2:28:11	+19:36:13	Ib	2006 Jan 11	CBET 364	CBET 368
SN 2006T	M14		9:54:30	-25:42:29	IIb	2006 Jan 30	IAUC 8666	IAUC 8680
SN 2006aj[1]	M14	Y	3:21:39	+16:52:02.6	Ic-BL	2006 Feb 18	IAUC 8674	CBET 409
SN 2006ba			9:43:13	-9:36:53	IIb	2006 Mar 19	IAUC 8693	CBET 458
SN 2006bf			12:58:50	+9:39:30	IIb	2006 Mar 19	IAUC 8693	M14
SN 2006cb			14:16:31	+39:35:15	Ib	2006 May 5	IAUC 8709	CBET 529
SN 2006ck[2]	M14		13:09:40	-1:02:57	Ic	2006 May 20	IAUC 8713	CBET 519
SN 2006el[2]	M14		22:47:38	+39:52:27.6	Ib	2006 Aug 25	IAUC 8741	CBET 612
SN 2006ep	M14		0:41:24	+25:29:46.7	Ib	2006 Aug 30	IAUC 8744	CBET 612
SN 2006fo[2]	M14	Y	2:32:38	+00:37:03.0	Ib	2006 Sep 16	IAUC 8750	M14
SN 2006gi[1]			10:16:46	73:26:26	Ib	2006 Sep 18	CBET 630	CBET 635
SN 2006ir			23:04:35	7:36:21	Ic	2006 Sep 24	CBET 658	Leloudas et al. 2011
SN 2006jc[1,2,e]	M14	Y	9:17:20	+41:54:32.7	Ib-n	2006 Oct 09	IAUC 8762	CBET 672/674/677
SN 2006lc	M14		22:44:24	-0:09:53	Ib	2006 Oct 25	CBET 693	CBET 699
SN 2006ld	M14	Y	0:35:27	+02:55:50.7	Ib	2006 Oct 19	IAUC 8766	CBET 689
SN 2006lv	M14		11:32:03	+36:42:03.6	Ib	2006 Oct 28	IAUC 8771	CBET 722
SN 2007C[2]	M14	Y	13:08:49	-6:47:01	Ib	2007 Jan 7	IAUC 8792	CBET 800
SN 2007D[2]	M14	Y	3:18:38	+37:36:26.4	Ic-BL	2007 Jan 7	IAUC 8794	CBET 805
SN 2007I	M14	Y	11:59:13	-1:36:18	Ic-BL	2007 Jan 14	IAUC 8798	CBET 808
SN 2007ag	M14		10:01:35	+21:36:42.0	Ib	2007 Mar 7	IAUC 8822	CBET 874
SN 2007aw			9:57:24	-19:21:23	Ic	2006 Mar 22	IAUC 8829	CBET 908
SN 2007bg[3,4]	M14		11:49:26	+51:49:28.8	Ic-BL	2007 Apr 16	IAUC 8834	CBET 927/948
SN 2007ce	M14	Y	12:10:17	+48:43:31.5	Ic-BL	2007 May 4	IAUC 8843	CBET 953
SN 2007cl	M14		17:48:21	+54:09:05.2	Ic	2007 May 23	IAUC 8851	CBET 974
SN 2007gr[1]	M14	Y	2:43:27	+37:20:44.7	Ic	2007 Aug 15	CBET 1034	CBET 1036
SN 2007hb	M14		2:08:34	+29:14:14.3	Ic	2007 Sep 24	CBET 1043	M14
SN 2007iq	M14		6:13:32	+69:43:49.2	Ic/Ic-BL	2007 Sep 12	CBET 1064	CBET 1101
SN 2007ke[1]			2:54:23	+41:34:16	Ib (Ca rich)	2007 Sep 25	CBET 1084	CBET 1101
SN 2007kj	M14		0:01:19	+13:06:30.6	Ib	2007 Oct 2	CBET 1092	CBET 1093
SN 2007ru[1]	M14		23:07:23	+43:35:33.7	Ic-BL	2007 Nov 30	CBET 1149	CBET 1151
SN 2007rz[6]	M14		4:31:10	+07:37:51.5	Ic	2007 Dec 8	CBET 1158	CBET 1160
SN 2007uy[1]	M14	Y	9:09:35	+33:07:08.9	Ib-pec	2007 Dec 31	IAUC 8908	M14
SN 2008D[1]	M14	Y	9:09:30	+33:08:20.3	Ib	2008 Jan 7	GCN 7159	CBET 1205
SN 2008an	M14		17:38:28	+61:02:13.7b	Ic	2008 Feb 24	CBAT 1268	CBAT 1271
SN 2008aq[7]	M14		12:50:30	-10:52:01	IIb	2008 Feb 27	CBAT 1271	CBAT 1271
SN 2008ax[1]	M14	Y*	12:30:40	+41:38:14.5	IIb	2008 Mar 3	CBET 1280/6	CBET 1298
SN 2008bo[6]	M14		18:19:54	+74:34:20.9	IIb	2008 Apr 1	CBET 1324	CBET 1325
SN 2008cw	M14		16:32:38	+41:27:33.2	IIb	2008 Jun 1	IAUC 1395	CBET 1408
SN 2008hh		Y*	1:26:03	11:26:26	Ic	2008 Nov 20	CBET 1575	CBET 1580
SN 2009K			4:36:36	-0:08:35.6	IIb	2009 Jan 14	CBET 1663	CBET 1665/1703
SN 2009er[f]	M14	Y	15:39:29	+24:26:05.3	Ib-pec	2009 May 22	CBAT 1811	M14
SN 2009iz	M14	Y	2:42:15	+42:23:50.1	Ib	2009 Sep 19	CBET 1943	M14
SN 2009jf[1]	M14	Y	23:04:52	+12:19:59.5	Ib	2001 Sep 17	IAUC 7719	IAUC 7721

Notes.
[1] Indicates SNe whose early-time behavior has been studied in the literature. [2]Included in the D11 sample.
[3] Radio studies, no published optical light curve. [4]Progenitor studies, no published light curve. [5]Host studies, no published light curve. [6]Only spectra published. [7]Only UV data published.
[a] These objects have spectra presented in M14.
[b] Object for which NIR data is available within the CfA survey. *Indicates *only* NIR data is available within the CfA survey for this object.
[c] SN reclassified with SNID using updated templates in M14 have the new classification reported.
[d] SN 2005la is spectroscopically peculiar showing narrow He and H lines in emission (Pastorello et al. 2008a).
[e] SN 2006jc is spectroscopically peculiar and showed narrow He lines in emission; see the text for details.
[f] The type classification of SN 2009er remains ambiguous. SNID classifies SN 2009er differently at different epochs. We also note the presence of high velocity He I lines.

Table 2
SN Host-galaxy Basic Data

SN Name	SN Type[a]	Galaxy[b]	$cz_{\rm helio}$[c] (km s^{-1})	$M_{\rm B}$[d] (mag)	$m_{\rm B}$[d] (mag)	$m - M$[d] (mag)	Morphology[d]	SN Offsets[e] (″)	(″)	E_{B-V}[f]
SN 2001ej	Ib	UGC 3829	4031	−20.46	13.44 (0.2)	33.90	Sb	4W	7N	0.0460
SN 2001gd	IIb	NGC 5033	1024	**−20.95**	**10.70 (0.13)**	**30.92**	**Sc**	52W	161N	0.0098
SN 2002ap	Ic-BL	M74	659	**−20.71**	**9.70 (0.26)**	**29.67**	**Sc**	258W	108S	0.0620
SN 2003jd	Ic-BL	MCG-01-59-21	5635	**−19.81**	**15.21 (0.50)**	34.42	**SABm**	8E	8S	0.0784
SN 2004ao	Ib	UGC 10862	1691	**−18.53**	**14.41 (0.59)**	32.15	**SBc**	6.3E	23.8S	0.0893
SN 2004aw	Ic	NGC 3997	4770	**−20.78**	**14.04 (0.13)**	34.48	**SBb**	28E	20S	0.0180
SN 2004fe	Ic	NGC 132	5363	**−21.13**	**13.74 (0.33)**	34.40	**SABb**	9E	12S	0.0210
SN 2004gk	Ic	IC 3311	−122	**−18.00**	**14.71 (0.18)**	**31.48**	**Scd**	2E	3N	0.0247
SN 2004gq	Ib	NGC 1832	1919	**−21.41**	**11.64 (0.52)**	**32.00**	**Sbc**	22E	22N	0.0627
SN 2004gt	Ic	NGC 4038	1663	**−21.45**	**10.85 (0.11)**	**31.72**	**SBm**	34W	10S	0.0398
SN 2004gv	Ib	NGC 0856	6017	**−20.78**	**14.21 (0.27)**	**34.69**	**Sa**	14W	4S	0.0276
SN 2005az	Ic	NGC 4961	2517	**−19.26**	**13.96 (0.06)**	**32.65**	**SBc**	8W	6N	0.0097
SN 2005bf	Ib	MCG+00-27-5	5670	**−21.53**	**13.60 (0.26)**	**29.67**	**Sc**	13E	32S	0.0385
SN 2005ek	Ic	UGC 2526	4962	**−21.29**	**15.38 (0.33)**	33.99	**Sc**	66E	60S	0.1788
SN 2005hg	Ib	UGC 1394	6388	**−21.10**	**14.66 (0.39)**	34.54	**Sa**	4W	20S	0.0901
SN 2005kf	Ic	SDSS J0747+2655[g]	4522	**−17.01**	**17.33 (0.29)**	-	-	1E	1S	0.0378
SN 2005kl	Ic	NGC 4369	1016	**−19.11**	**12.36 (0.11)**	31.67	**Sa**	6W	4N	0.0219
SN 2005kz	Ic	MCG+08-34-32	8107	**−20.83**	**15.19 (0.33)**	35.33	**SBa**	15.6E	9.5N	0.0460
SN 2005la	Ib/IIb	PGC 043632	5570	**−18.43**	**16.67 (0.50)**	34.62	**Sc**	6W	6S	0.0100
SN 2005mf	Ic	UGC 4798	8023	**−20.34**	**15.34 (0.32)**	35.49	**Sc**	6W	13N	0.0153
SN 2005nb	Ic-BL	UGC 7230	7127	−21.13	14.05 (0.2)	35.18	SB(s)d pec	2W	5N	0.0320
SN 2006F	Ib	NGC 935	4197	**−21.39**	**13.75 (0.41)**	33.44	**Sc**	3E	15N	0.1635
SN 2006T	IIb	NGC 3054	2396	**−20.95**	**12.34 (0.14)**	**32.68**	**Sb**	22E	21S	0.0647
SN 2006aj	Ic-BL	Anonymous	10052	-	-	-	-	-	-	0.1267
SN 2006ba	IIb	NGC 2980	5764	**−21.78**	**13.60 (0.04)**	34.48	**Sc**	21E	8S	0.0452
SN 2006bf	IIb	UGC 8093	7115	**−20.82**	**14.92 (0.27)**	35.18	**Sbc**	3.1W	15.5N	0.0216
SN 2006cb	Ib	NGC 5541	7708	**−21.84**	**13.89 (0.58)**	35.30	**Sc**	0.6E	5.7S	0.0094
SN 2006ck	Ic	UGC 8238	7312	**−20.86**	**14.95 (0.36)**	35.24	**Sc**	10W	3S	0.0245
SN 2006el	Ib	UGC 12188	5150	-	14.4 (0.4)	-	S+companion	13E	18S	0.0973
SN 2006ep	Ib	NGC 214	4505	**−21.65**	**12.94 (0.05)**	33.86	**SABc**	43W	11S	0.036
SN 2006fo	Ib	UGC 2019	6214	**−20.36**	**14.81 (0.47)**	34.69	**Sbc**	14E	4N	0.0250
SN 2006gi	Ib	NGC 3147	2780	**−22.22**	**11.26 (0.15)**	**32.99**	**Sbc**	30W	144N	0.0205
SN 2006ir	Ic	PGC 085376	6220	-	**17.36 (0.50)**	34.63	-	-	-	0.0393
SN 2006jc	Ib-n	UGC 4904	1644	**−17.47**	**15.05 (0.35)**	**32.99**	**SBbc**	11W	7S	0.0173
SN 2006lc	Ib	NGC 7364	4863	**−21.24**	**13.44 (0.43)**	33.87	**S0-a**	1E	10S	0.0556
SN 2006ld	Ib	UGC 348	4179	**−18.44**	**15.86 (0.39)**	33.71	**SABd**	1E	18S	0.0144
SN 2006lv	Ib	UGC 6517	2490	**−19.33**	**14.12 (0.46)**	32.99	**SBbc**	10E	12N	0.0245
SN 2007C	Ib	NGC 4981	1767	**−20.31**	**12.07 (0.30)**	**31.71**	**Sbc**	9E	22S	0.0363
SN 2007D	Ic-BL	UGC 2653	6944	**−21.70**	**15.68 (0.50)**	35.08	**Scd**	5E	3S	0.2881
SN 2007I	Ic-BL	PGC 1114807	6487	**−16.77**	**18.30 (0.25)**	34.99	-	-	-	0.0250
SN 2007ag	Ib	UGC 5392	6017	**−20.33**	**15.94 (0.35)**	35.30	Scd(?)	4E	16N	0.0250
SN 2007aw	Ic	NGC 3072	3431	**−19.91**	**13.83 (0.19)**	33.68	**S0-a**	3.3E	5.2S	0.0338
SN 2007bg	Ic-BL	Anonymous	10370	-	-	-	-	-	-	0.0179
SN 2007ce	Ic-BL	Anonymous	13890	-	-	-	-	-	-	0.0200
SN 2007cl	Ic	NGC 6479	6650	**−20.85**	**14.50 (0.33)**	34.90	**Sc**	3W	8N	0.0200
SN 2007gr	Ic	NGC 1058	518	**−18.70**	**11.96 (0.14)**	29.28	**Sc**	25W	16N	0.0535
SN 2007hb	Ic	NGC 819	6669	**−20.90**	**16.23 (0.35)**	34.91	S(?)	19W	5S	0.0518
SN 2007iq	Ic/Ic-BL	UGC 3416	4003	**−20.19**	**15.08 (0.32)**	33.59	**Sc**	39W	30S	0.1182
SN 2007ke	Ib (Ca rich)	NGC 1129	5194	**−21.64**	**13.40 (0.72)**	34.30	**E**	39.1W	29.8S	0.0954
SN 2007kj	Ib	NGC 7803	5366	**−20.92**	**13.08 (0.11)**	34.34	**S0-a**	6W	10S	0.0691
SN 2007ru	Ic-BL	UGC 12381	4636	**−20.37**	**15.12 (0.44)**	33.99	**Sc**	5E	41S	0.2254
SN 2007rz	Ic	NGC 1590	3897	**−20.25**	**14.49 (0.04)**	33.71	**Sc B**	9E	0N	0.1723
SN 2007uy	Ib-pec	NGC 2770	2100	**−20.78**	**12.76 (0.05)**	**32.08**	**SABc**	21E	15S	0.0194
SN 2008D	Ib	NGC 2770	2100	**−20.78**	**12.76 (0.05)**	**32.08**	**SABc**	38W	56N	0.0194
SN 2008an	Ic	UGC 10936	8124	**−20.79**	**15.36 (0.49)**	35.35	**Sb**	5E	10S	0.0450
SN 2008aq	IIb	MCG-02-33-20	2389	-	13.27 (0.15)	32.45	SB(s)m	15E	45S	0.0383
SN 2008ax	IIb	NGC 4490	630	**−21.82**	**9.76 (0.17)**	**29.90**	**SBcd**	15E	45S	0.0186
SN 2008bo	IIb	NGC 6643	1484	**−21.10**	**11.76 (0.08)**	**31.57**	**Sc**	31E	15N	0.0513
SN 2008cw	IIb	PGC 2181396	9724	**−18.34**	**17.60 (0.47)**	-	-	1E	2N	0.0060
SN 2008hh	Ic	IC 112	5819	**−21.23**	**14.16 (0.41)**	34.51	**Sd**	9.8E	8.4S	0.0427
SN 2009K	IIb	NGC 1620	3530	**−21.82**	**12.87 (0.21)**	33.07	**SABc**	8.7W	1.5N	0.0499
SN 2009er	Ib-pec	SDSS J1539+2426[h]	10500	**−18.22**	**18.05 (0.50)**	35.87	-	8W	9S	0.0389
SN 2009iz	Ib	UGC 02175	4257	**−21.82**	**12.87 (0.21)**	33.84	**SABc**	12W	14N	0.0729
SN 2009jf	Ib	NGC 7479	2443	**−19.00**	**15.60 (0.32)**	32.64	**SABb**	54W	36N	0.0971

Notes.
[a] The SN Type "Ic-BL" stands for broad-lined SN Ic. SN 2006jc is a SN Ib-n ("n" for narrow) which showed narrow He lines in emission. See text for details.
[b] "Anonymous" stands for non-catalogued host galaxy.
[c] From NED catalog.
[d] From HyperLEDA catalog (bold) or NED catalog.
[e] From http://www.cbat.eps.harvard.edu/lists/Supernovae.html.
[f] Galactic extintion calculated according to Schlafly & Finkbeiner (2011)
[g] Abbreviated galaxy name for SDSS J074726.40+265532.4.
[h] Abbreviated galaxy name for SDSS J153930.49+242614.8.

Table 3
SN 2005hg Comparison Optical Photometry

Star	R.A.(J2000)	Decl.(J2000)	V	N_V	$U-B$	N_U	$B-V$	N_B	$V-r'$	$N_{r'}$	$V-i'$	$N_{i'}$
01	01:56:08.386	+46:51:51.91	16.217 ± .013	3	0.113 ± .052	3	0.729 ± .020	3	0.189 ± .009	3	0.407 ± .011	3
02	01:56:03.007	+46:52:47.44	16.338 ± .013	3	0.382 ± .043	3	0.740 ± .016	3	0.204 ± .011	3	0.395 ± .011	3
03	01:56:02.641	+46:52:31.82	16.032 ± .012	3	0.091 ± .042	3	0.593 ± .017	3	0.150 ± .010	3	0.314 ± .011	3
04	01:56:02.558	+46:43:25.08	15.460 ± .012	3	0.170 ± .042	3	0.725 ± .015	3	0.192 ± .009	3	0.381 ± .009	3
05	01:55:59.139	+46:51:51.01	15.467 ± .012	3	0.102 ± .047	3	0.620 ± .017	3	0.159 ± .011	3	0.330 ± .010	3
06	01:55:59.060	+46:46:57.56	15.492 ± .013	3	0.250 ± .056	3	0.759 ± .017	3	0.211 ± .009	3	0.431 ± .009	3
07	01:55:58.585	+46:49:29.73	15.898 ± .013	3	0.105 ± .050	3	0.632 ± .016	3	0.166 ± .011	3	0.344 ± .009	3
08	01:55:57.677	+46:44:26.44	14.789 ± .013	3	0.095 ± .043	3	0.603 ± .016	3	0.135 ± .010	3	0.264 ± .009	3
09	01:55:57.102	+46:42:17.85	15.387 ± .012	3	0.337 ± .099	3	0.841 ± .055	3	0.215 ± .009	3	0.417 ± .028	3
10	01:55:57.103	+46:49:56.47	15.740 ± .013	3	0.117 ± .044	3	0.601 ± .016	3	0.146 ± .010	3	0.302 ± .009	3
11	01:55:57.059	+46:52:27.68	15.967 ± .013	3	0.105 ± .045	3	0.575 ± .017	3	0.136 ± .010	3	0.279 ± .009	3
12	01:55:52.143	+46:46:55.57	15.723 ± .013	3	0.333 ± .044	3	0.721 ± .016	3	0.181 ± .009	3	0.332 ± .009	3
13	01:55:45.171	+46:47:37.72	15.207 ± .013	3	−0.018 ± .044	3	0.502 ± .018	3	0.114 ± .009	3	0.232 ± .009	3
14	01:55:43.728	+46:45:15.07	16.674 ± .015	3	0.192 ± .044	3	0.646 ± .021	3	0.157 ± .018	3	0.275 ± .012	3
15	01:55:42.395	+46:50:57.27	16.022 ± .012	3	0.068 ± .043	3	0.614 ± .016	3	0.151 ± .010	3	0.306 ± .009	3
16	01:55:41.672	+46:42:26.85	15.505 ± .056	3	0.075 ± .071	3	0.573 ± .017	3	0.134 ± .011	3	0.300 ± .030	3
17	01:55:39.694	+46:48:48.36	14.894 ± .013	3	0.802 ± .043	3	1.010 ± .016	3	0.310 ± .009	3	0.608 ± .009	3
18	01:55:38.790	+46:51:18.19	15.114 ± .013	3	0.000 ± .042	3	0.506 ± .015	3	0.116 ± .009	3	0.237 ± .010	3
19	01:55:34.046	+46:50:11.12	16.249 ± .014	3	0.035 ± .046	3	0.645 ± .016	3	0.165 ± .009	3	0.356 ± .010	3
20	01:55:30.653	+46:47:13.56	15.956 ± .012	3	0.012 ± .046	3	0.628 ± .015	3	0.155 ± .011	3	0.325 ± .010	3
21	01:55:20.903	+46:51:07.29	14.712 ± .013	3	0.572 ± .042	3	0.942 ± .016	3	0.287 ± .009	3	0.585 ± .009	3
22	01:55:14.253	+46:45:00.08	16.515 ± .015	2	0.012 ± .045	2	0.611 ± .016	2	0.141 ± .009	2	0.301 ± .011	3
23	01:55:10.188	+46:50:01.06	16.070 ± .108	2	−0.243 ± .128	2	0.576 ± .079	2	0.164 ± .016	2	0.402 ± .102	3

Note. The natural system values can be calculated by applying the color terms or are available upon request.

(This table is available in its entirety in a machine-readable form in the online journal. A portion is shown here for guidance regarding its form and content.)

3. PHOTOMETRY DATA AND REDUCTION

Our optical and NIR photometric campaigns are described in detail below and elsewhere (Hicken et al. 2009, 2012; Wood-Vasey et al. 2008; A. S. Friedman et al. 2014, in preparation). We paid particular attention to removing galaxy contamination, as contaminating host-galaxy light may affect both the estimates of the peak brightness of the SN and its decline rate (Boisseau & Wheeler 1991). The optical sample is produced from template-subtracted images in all but six cases where the SN is well removed from the host galaxy (Section 3.1). Thus, ∼90% of our optical sample of 64 stripped SNe have photometry based on template-subtracted images. Similarly, for 80% of our objects with NIR coverage, NIR photometry is derived from template-subtracted images: all but 5 objects out of 25.

Photometry in both the natural and standard system is available in the supplementary material of this paper, as well as through the CfA Web site.[12]

Below we describe the photometry acquisition for both optical and NIR photometry as well as the image and photometric reduction pipelines.

3.1. Optical Photometric Observations and Reductions

All optical photometry presented in this paper was obtained with the FLWO 1.2 m telescope during the CfA3 (Hicken et al. 2009) and CfA4 campaigns (Hicken et al. 2012). Three different cameras were used to acquire the photometry: the 4Shooter 2 × 2 CCD mosaic (for data before 2004 September), the Minicam CCD mosaic camera (2004 September until 2005 July), and the Keplercam CCD mosaic camera (after 2005 August). All cameras are thinned, back-illuminated CCDs, mounted at the $f/8$ Cassegrain focus of the 1.2 m telescope. All UBV photometry is obtained in Johnson UBV, with B and V Harris filters. At redder wavelengths, observations were conducted with the 4Shooter 2 × 2 CCD mosaic in Johnson RI band passes with the Harris filter set and after 2004 September with Sloan Digital Sky Survey (SDSS) $r'i'$ filters (Fukugita et al. 2007; Smith et al. 2002). In addition, in 2009 January the Johnson U filter broke and was replaced by an SDSS u' filter. Two objects in our survey, SN 2009iz and SN 2009jf, have u' data. The typical FWHM in our data falls between 1.″5 and 3″, with the larger values typically found in the CfA4 survey. To provide prompt and dense sampling, the SNe were observed by observers at the telescopes for other programs and supplemented by photometric observations on our scheduled nights.

The optical photometry presented here was produced at the same time and in the same way as the CfA3 and CfA4 SNe Ia samples. The detailed operations of the optical photometric pipeline are discussed in Hicken et al. (2009, 2012). In brief, we employed differential photometry by measuring the brightness of the SNe with respect to a set of comparison stars (ranging from a few to dozens) in the SN field. We employed the photometry pipeline of the SuperMACHO and ESSENCE collaborations (see Rest et al. 2005 and Miknaitis et al. 2007 for details) adapted for the 1.2 m FLWO.

A finding chart is shown in Figure 1, with the field comparison stars marked. Comparison stars for each SN are available on the Web,[13] and the photometry for the comparison stars used to produce the optical light curve of SN 2005hg is shown, as an example, in Table 3. The comparison stars were calibrated on photometric nights by observing standard stars from Landolt (1992) and Smith et al. (2002). Aperture photometry in IRAF[14] was used for this calibration.

[12] http://www.cfa.harvard.edu/oir/Research/supernova/

[13] http://www.cfa.harvard.edu/oir/Research/supernova/

[14] IRAF (Image Reduction and Analysis Facility) is written and supported by the National Optical Astronomies Observatories, which are operated by the Association of Universities for Research in Astronomy, Inc., under cooperative agreement with the National Science Foundation.

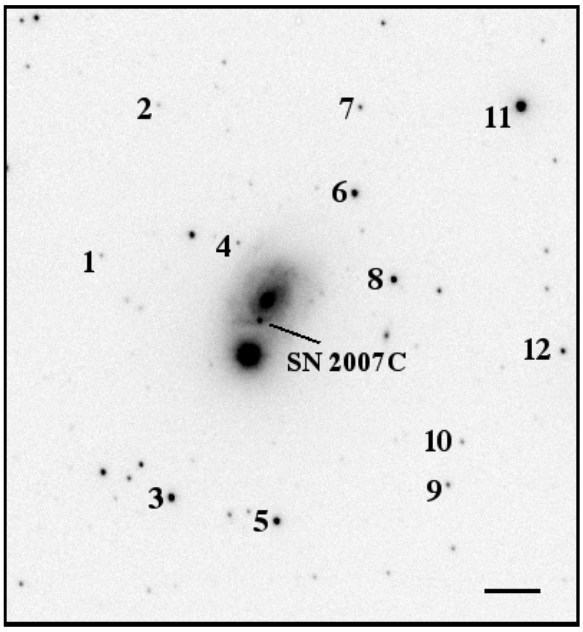

Figure 1. Example supernova finding chart. This image of SN 2007C was collected with Keplercam on the FLWO 1.2 m telescope (http://linmax.sao.arizona.edu/FLWO/48/kep.primer.html) on 2007 January 21. The comparison stars are indicated with numbers from 1 to 12. North is top and east is to the left. The bar in the lower right corner indicates 1′.

Color terms are obtained from the standard stars. The implicit color term equations have the following form: for Keplercam-chip2/Sloan, for example, $(v - r) = 1.0458(V - r')$+constant. For the $UBVRI$ filters, the lowercase/uppercase letters in the color terms refer to instrumental/standard magnitudes. For the $u'r'i'$ filters, the lowercase letters refer to the instrumental magnitudes, whereas the primed lowercase letters refer to the standard magnitudes. Average color terms for each setup used in our optical sample, along with the internal uncertainties in the mean, are available in Table 4.[15]

Throughout the survey, five different sets of color terms were used, corresponding to four different camera/filter setups (4Shooter 2 × 2 – $UBVRI$, Minicam – $UBVr'i'$, Keplercam – $UBVr'i'$, and Keplercam – $u'BVr'i'$), slight modifications to the photometric pipeline between CfA3 and CfA4 (all 4Shooter, Minicam and much of the Keplercam data before 2009 was processed during CfA3 while some of the data before 2009 and all of it afterward was processed during CfA4), and lastly, changes in the instrument transmission observed in mid-2009. For each light curve made available online (see Tables 5 and 6), a reduction code that identifies both instrument setup and pipeline used for the reduction is indicated in the file header as CfA3_4SH/$UBVRI$, CfA3_MINI/$UBVr'i'$, CfA3_KEP/$UBVr'i'$, CfA4_KEP1/$UBVr'i'$, and CfA4_KEP2/$u'BVr'i'$, linking the data to the correct set of color terms to be used for photometric transformations. Anyone wishing to use the natural system passbands must ensure that the proper passband is used to correct the photometry.

With the exception of six objects that are well removed from the host galaxy (SN 2002ap, SN 2004aw, SN 2006gi, SN 2007ce, SN 2007ru, and SN 2008aq), we derive photometric measurements from template-subtracted images (see Smith et al. 2002) using the robust algorithm of Alard & Lupton (1998; also discussed in Alard 2000). The template images of SN host galaxies were obtained under optimal seeing conditions, after the SN had faded sufficiently, usually 6 months to 1 yr after the end of the SN observing campaign. In Table 2 we report the characteristics of the host galaxies for all objects in our sample.

DoPHOT point-spread function (PSF) photometry (Schechter et al. 1993) was used to measure the flux of a SN and

[15] http://www.cfa.harvard.edu/oir/Research/supernova/

Table 4
CfA3 and CfA4 Photometric Color Terms

Detector/Filters	Color Term	Value
Before 2004 September (CfA3_4SH)		
4Shooter/$UBVRI$	$(u - b)/(U - B)$	0.9912 ± 0.0078
4Shooter/$UBVRI$	$(b - v)/(B - V)$	0.8928 ± 0.0019
4Shooter/$UBVRI$	$(v - V)/(B - V)$	0.0336 ± 0.0020
4Shooter/$UBVRI$	$(v - r)/(V - R)$	1.0855 ± 0.0058
4Shooter/$UBVRI$	$(v - i)/(V - I)$	1.0166 ± 0.0067
Between 2004 September and 2005 July (CfA3_MINI)		
Minicam/$UBVr'i'$	$(u - b)/(U - B)$	1.0060 ± 0.0153
Minicam/$UBVr'i'$	$(b - v)/(B - V)$	0.9000 ± 0.0095
Minicam/$UBVr'i'$	$(v - V)/(B - V)$	0.0380 ± 0.0030
Minicam/$UBVr'i'$	$(v - r)/(V - r')$	1.0903 ± 0.0140
Minicam/$UBVr'i'$	$(v - i)/(V - i')$	1.0375 ± 0.0088
Between 2005 August and 2009 July—CfA3 (CfA3_KEP)		
Keplercam/$UBVr'i'$	$(u - b)/(U - B)$	1.0279 ± 0.0069
Keplercam/$UBVr'i'$	$(b - v)/(B - V)$	0.9212 ± 0.0029
Keplercam/$UBVr'i'$	$(v - V)/(B - V)$	0.0185 ± 0.0023
Keplercam/$UBVr'i'$	$(v - r)/(V - r')$	1.0508 ± 0.0029
Keplercam/$UBVr'i'$	$(v - i)/(V - i')$	1.0185 ± 0.0020
Between 2005 August and 2009 July—CfA4 (CfA4_KEP1)		
Keplercam/$UBVr'i'$	$(u - b)/(U - B)$	0.9981 ± 0.0109
Keplercam/$UBVr'i'$	$(b - v)/(B - V)$	0.9294 ± 0.0026
Keplercam/$UBVr'i'$	$(v - V)/(B - V)$	0.0233 ± 0.0018
Keplercam/$UBVr'i'$	$(v - r)/(V - r')$	1.0684 ± 0.0028
Keplercam/$UBVr'i'$	$(v - i)/(V - i')$	1.0239 ± 0.0016
After 2009 July (CfA4_KEP2)		
Keplercam/$u'BVr'i'$	$(u - b)/(u - B)$	0.9089 ± 0.0057
Keplercam/$u'BVr'i'$	$(b - v)/(B - V)$	0.8734 ± 0.0024
Keplercam/$u'BVr'i'$	$(v - V)/(B - V)$	0.0233 ± 0.0018
Keplercam/$u'BVr'i'$	$(v - r)/(V - r')$	1.0265 ± 0.0033
Keplercam/$u'BVr'i'$	$(v - i)/(V - i')$	1.0239 ± 0.0016

Notes. Lower-case $ubvri$ refer to the instrumental magnitudes while $u'UBVRIr'i'$ refer to the standard magnitudes. All color terms implicitly contain an additive constant. For example, for the Keplercam $(v-V) = 0.0185(B-V)$ + const; $(u - b) = 1.0279(U - B)$ + const.

Table 5
SN Optical and NIR Photometry in the Natural System

SN	Filter	MJD (d)	Mag ((mag))	σ_{mag} ((mag))	Code
2001ej	B	52188.42804	17.861	0.041	CfA3_4SH
2001ej	B	52206.47248	19.175	0.044	CfA3_4SH
2001ej	B	52226.47150	19.579	0.072	CfA3_4SH
2001ej	B	52227.51045	19.574	0.064	CfA3_4SH
2001ej	B	52228.50909	19.639	0.064	CfA3_4SH
2001ej	B	52257.42124	20.002	0.099	CfA3_4SH
2001ej	B	52266.42038	19.836	0.086	CfA3_4SH
2001ej	B	52267.45358	19.820	0.080	CfA3_4SH

(This table is available in its entirety in a machine-readable form in the online journal. A portion is shown here for guidance regarding its form and content.)

Table 6
SN Optical and NIR Photometry in the Standard System

SN	Filter	MJD (d)	Mag ((mag))	σ_{mag} ((mag))	Code
2001ej	*B*	52188.42804	17.915	0.041	CfA3_4SH
2001ej	*B*	52206.47248	19.265	0.044	CfA3_4SH
2001ej	*B*	52226.47150	19.672	0.072	CfA3_4SH
2001ej	*B*	52227.51045	19.665	0.064	CfA3_4SH
2001ej	*B*	52228.50909	19.737	0.064	CfA3_4SH
2001ej	*B*	52257.42124	20.083	0.099	CfA3_4SH
2001ej	*B*	52266.42038	19.897	0.086	CfA3_4SH
2001ej	*B*	52267.45358	19.879	0.080	CfA3_4SH

(This table is available in its entirety in a machine-readable form in the online journal. A portion is shown here for guidance regarding its form and content.)

its comparison stars. The majority of the stripped SN photometry in this work was produced during the CfA3 campaign and used only one host-galaxy image for host subtraction. However, the CfA4 campaign used multiple host-galaxy images where possible, and for stripped SN produced during CfA4 we use the median photometry pipeline uncertainty as the uncertainty for each light curve point. The CfA4 SNe Ia uncertainties (Hicken et al. 2012) also added, in quadrature, the standard deviation of the photometry values from the multiple host-image subtractions for a given point to produce the total uncertainty. However, this overestimates the uncertainty (Scolnic et al. 2013). In order to maintain consistency with the CfA3-era stripped SNe, we present the CfA4 data without adding the standard deviation to the CfA4-era uncertainties. The optical photometry of the 61 SNe is available for download[16] and in the supplementary material for this paper.

Optical CfA photometry of some of the SNe listed in this paper has been previously published: SN 2005bf (Tominaga et al. 2005), SN 2006aj/GRB060218 (Modjaz et al. 2006), and SN 2008D (Modjaz et al. 2009). The optical data previously published for SN 2005bf were not based on template-subtracted images. Although SN 2005bf is well removed from its host, so host contamination was not significant. Here we present the template-subtracted photometry, produced with the standard CfA photometric pipeline. Thus, the light curves presented here for SN 2005bf supersede those previously published.

CfA photometry for four objects, spanning the best and worst sampling quality, is shown in Figure 2. Note that for SN 2005hg, SN 2009iz, and SN 2006ep, where the epoch of maximum *V*-band brightness is known (see Section 4), the epochs are expressed both as JD (bottom *x*-axis) and as days since/to *V*-band peak (top *x*-axis). However, the epoch of maximum *V*-band brightness is *not* known for SN 2008an. Plots for all SN are available online.[17]

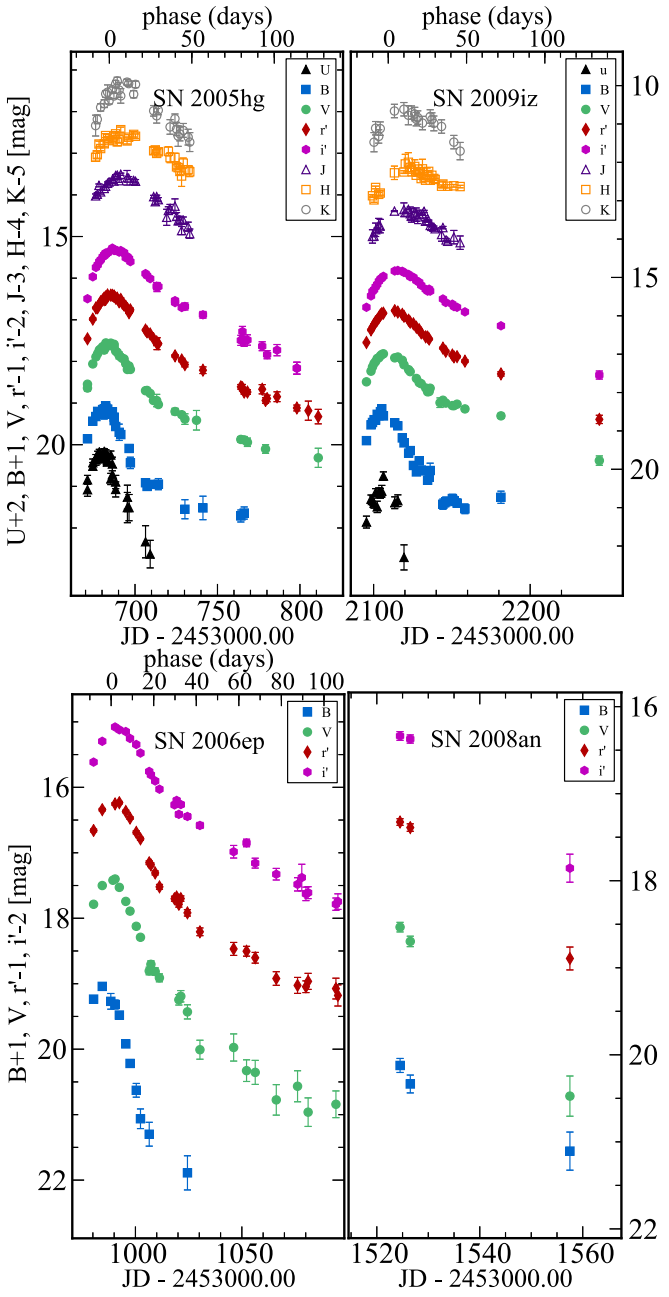

Figure 2. Optical and NIR photometry of four SNe chosen to represent the range of wavelength and cadence coverage in our sample. The multi-color light curves in *U* (black triangles), *B* (blue squares), *V* (green circles), r' (red diamonds), i' (magenta hexagons), *J* (purple empty triangles), *H* (orange empty squares), and K_s (gray empty circles) light curves are shown with offsets as indicated on the *y*-axis.

(A color version of this figure is available in the online journal.)

3.2. Near-infrared Photometry

For 25 SNe in our sample, we obtained NIR photometry with the fully automated 1.3 m PAIRITEL[18] located at FLWO. PAIRITEL is a refurbishment of the Two Micron All Sky Survey (2MASS) North telescope outfitted with the 2MASS South camera (Skrutskie et al. 2006) and is the first fully robotic and dedicated IR imaging system for the follow-up of transients (Bloom et al. 2006). The automation of PAIRITEL has enabled NIR SNe with simultaneous *J*-, *H*-, and K_s-band observations and nearly nightly cadence allows for densely sampled PAIRITEL NIR SNe light curves from as many as ~10 days before *V*-band maximum brightness to ~150 days past maximum. PAIRITEL SNe Ia data are published in Wood-Vasey et al. (2008), Friedman (2012), and A. S. Friedman et al. (2014, in preparation) will present the CfAIR2 sample of ~100 JHK_s SNe Ia light curves.

PAIRITEL data for individual stripped-envelope SNe have been published in Tominaga et al. (2005), Kocevski et al. (2007),

[16] http://www.cfa.harvard.edu/oir/Research/supernova/
[17] http://www.cosmo.nyu.edu/SNYU
[18] http://www.pairitel.org/

Modjaz et al. (2009), Marion et al. (2014), and Drout et al. (2013).

PAIRITEL *J*-, *H*-, and K_s-band images were acquired simultaneously with the three NICMOS3 arrays in double correlated reads with individual exposure times of 7.8 s. Individual images were dithered every fourth exposure in order to remove bad pixels and aid subtraction of the bright NIR sky. Each image consists of a 256 × 256 array with a plate scale of $2''$ pixel^{-1}, yielding an individual FOV of $8\farcm5 \times 8\farcm5$.

Sky subtraction is a crucial step in NIR image processing. The PAIRITEL image reduction pipeline software (Bloom et al. 2006; Wood-Vasey et al. 2008; Friedman 2012) performed sky subtraction before cross-correlating, stacking, and subsampling the processed images in order to produce the final, Nyquist-sampled image, with an effective pixel scale of $1''$ pixel^{-1}.

The PAIRITEL imager does not have a shutter, thus, independent determination of the dark current is impossible. For all SNe, the sky+dark values for a given raw image were determined using a star-masked, pixel-by-pixel robust average through a temporal stack of unregistered raw images, which included removing the highest and lowest pixel values in the stack. The temporal range of the raw image stack was set to ±5 minutes around the raw science image, which implicitly assumes that sky+dark values are approximately constant on ∼10 minute time scales. This reconstructed sky+dark image was then subtracted from the corresponding raw science image. For some SN fields with large host galaxies filling a fraction of the final FOV greater than ∼1/5, a pixel-by-pixel robust average through the image series can lead to biased sky+dark values due to excess galaxy light falling in those pixels. However, overall systematic effects are negligible, biasing photometry to be fainter by only ∼1–2 hundredths of a magnitude. The same sky+dark procedure was applied to all SN fields, including those with large host galaxies. The sky+dark subtracted dithered science images are then registered and combined into final mosaicked images with SWarp (Bertin et al. 2002), with an FOV of $12' \times 12'$.

Collection time ranged between 1800 s and 5400 s including overhead; the effective exposure times for the final mosaicked images ranged between 10 and 20 minutes. The effective seeing generally fell between $2''$ and $2\farcs5$ FWHM. The typical 30 minute signal-to-noise-ratio (S/N = 10) sensitivity limits are ∼18, 17.5, and 17 mag for *J*, *H*, and K_s, respectively. For fainter sources, 10σ point source sensitivities of 19.4, 18.5, and 18 mag are achievable with 1.5 hr of dithered imaging (Bloom et al. 2003).

Photometric data points are calculated using forced DoPHOT photometry at the best fit SN centroid position. Photometry is generated for each SN from both unsubtracted and template-subtracted mosaicked images, the latter produced using the ESSENCE pipeline (Rest et al. 2005). Typically, a minimum of three template images were obtained for each SN, after the SN had faded below our detection limit, 6 to 12 months after discovery. The template-subtracted light curves are created as a nightly weighted average of the photometry produced using different templates. The most reliable photometry is ultimately chosen by visual inspection of the unsubtracted and subtracted mosaicked images, as well as considering the scatter in the photometric measurement obtained by each method. For template-subtracted light curves, a combination of automated and visual inspection also allowed removal of individual bad subtractions and outlier data points arising from poor quality science or template images.

For SN not embedded in the host-galaxy nucleus, or with little host-galaxy light at the SN position, forced DoPHOT photometry on the un-subtracted mosaics was sometimes of higher quality than the galaxy subtracted light curves. We include in our sample forced photometry NIR light curves from *un-subtracted* images for the following objects: SN 2004gq, SN 2005ek, SN 2007ce, SN 2007uy, and SN 2008hh. All other NIR SN light curves included here used photometry on the template-subtracted images, including SN 2006aj, and SN 2008D, for which PAIRITEL photometry is already published in Kocevski et al. (2007) and Modjaz (2007), and Modjaz et al. (2009), respectively. A new light curve, generated from template-subtracted images, is presented here for SN 2005bf, and supersedes previously published PAIRITEL data in Tominaga et al. (2005). SN 2005ek is well separated from the host galaxy; the light curve presented here is not based on host subtracted images, however, we present additional PAIRITEL data points, together with those already included in Drout et al. (2013), and originally published in Modjaz (2007).

For each SN field, the SN brightness was determined using differential photometry against reference field stars in the 2MASS point source catalog (Cutri et al. 2003). Each field had ∼10–90 2MASS stars (which achieved 10σ point source sensitivities of $J = 15.8$ mag, $H = 15.1$ mag, $K_s = 14.3$ mag; Skrutskie et al. 2006). No color-term corrections were required since our natural system photometry is already on the 2MASS system. We extensively tested the accuracy and precision of both the PAIRITEL reduction and our photometry pipeline by comparing our photometry of 2MASS stars in the SN observations to that in the 2MASS catalog. The difference between the two photometry values is consistent with zero everywhere in the magnitude range $J = 12$–18 mag. Thus, we conclude our photometry is well anchored in the 2MASS system. Note, however, that the difference uncertainties are expected to be correlated since the 2MASS photometry values were used to compute the zero point of each image in the first place. More details of the PAIRITEL image processing and photometric pipelines are presented in Modjaz (2007), Wood-Vasey et al. (2008), Friedman (2012), and A. S. Friedman et al. (2014, in preparation).

NIR photometry is shown in Figure 2 for SN 2005hg and SN 2009iz.

4. CfA STRIPPED SN SAMPLE STATISTICS

The sample of stripped SN we present contains a total of 64 SN observed between 2001 and 2009. The quality varies. The list below details our objects grouped based on their photometric quality. Several objects are then discussed in the later sections of this paper.

1. Our best quality subset contains light curves in at least four bands with data before and after the *V* photometric peak. In this subset are multi-band light curves of 24 objects, 11 SNe Ib, 5 SNe Ic, 3 SNe IIb, 3 SNe Ic-BL, and 2 peculiar SNe Ib (SN 2007uy and SN 2009er).
2. An intermediate quality subsample contains multi-band light curves of 26 SNe: 6 SNe Ib, 8 SNe Ic, 4 SNe IIb, 4 SNe Ic-BL, 1 SN Ic/Ic-BL (SN 2007iq), 2 SNe Ib-n/IIb-n (Ib with narrow emission lines of H and He: SN 2005la and SN 2006jc), and 1 Ca-rich Ib (SN 2007ke).
3. Another subset contains 11 SN light curves for which we could not set good constraints on the date of maximum in any band or which contains only a few epochs or less than four photometric bands.

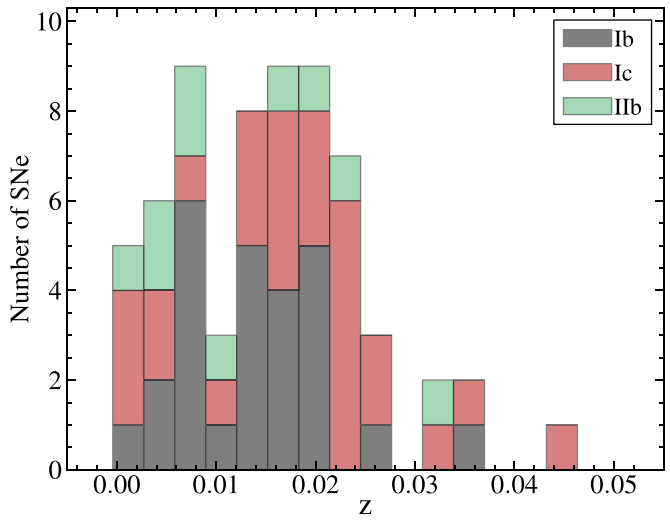

Figure 3. Redshift distribution of SNe in our sample. Each color represents a SN type: SNe Ib, Ic/Ic-BL, and IIb. The histograms are stacked: for each bin the total height of the bar indicates the total number of objects and the color segments represent the contribution of types within that redshift bin.

(A color version of this figure is available in the online journal.)

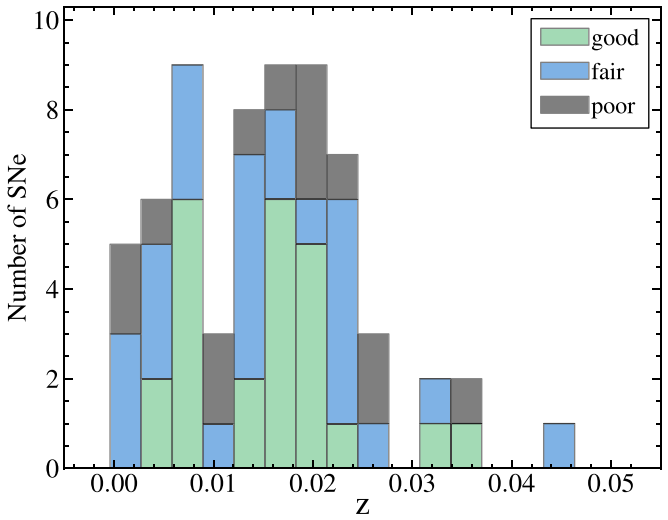

Figure 4. Same as Figure 3, but with the sample split by photometric quality, as described in Section 4 (good, fair, and poor light curve quality).

(A color version of this figure is available in the online journal.)

4. Finally, three objects (SN 2005ek, SN 2008ax, and SN 2008hh) have only NIR photometry.

The distribution of our objects in redshift is shown in Figure 3 where we identify different SN types with different colors and Figure 4 where the color indicates the quality of our photometry.

Most of the optical photometric measurements are in B, V, r', and i': 854, 1120, 1115, 1123 in each band, respectively; 183 measurements were collected in the U band. In addition, the earliest objects observed within our program (SN 2001ej, SN 2001gd, SN 2002ap, SN 2003jd, SN 2004ao, and SN 2004aw) were imaged with R and I filters, in place of r' and i', with 68 and 60 points in each band for the six objects. In 2009, the Johnson U filter was replaced by an SDSS u' filter; two objects, SN 2009iz and SN 2009jf, have u'-band data, a total of 20 data points, 13 for SN 2009iz and 7 for SN 2009jf. In the NIR we collected 774 measurements in J, 738 in H, and 630 in K_s. The photometry for each of our SN is made available as machine-readable tables in the online journal, on our Web site[19] as plots, and in tabular form.[20] In Table 7–9 we present observational photometric characteristics for all objects in our sample: the epoch of maximum brightness, the peak magnitude, and the decline rate in each filter whenever it is possible to derive them. Similarly to what is done for SNe Ia, we measure the decline rate as Δm_{15}: the difference in magnitude between peak and 15 days after peak. We simply rely on a second-degree polynomial fit near the light curve peak to obtain these quantities. Note that these are presented as observational quantities: no S- or K-corrections are applied to compensate for the reddening effects of redshift, nor do we correct for dust extinction at this time. A more complete analysis of our photometric data will be presented in a companion paper (F. B. Bianco et al., in preparation), and such corrections will be discussed there. The maximum brightness and the epoch of maximum are measured as follows.

1. For each single-band light curve we select by eye, a region around the peak large enough to allow a quadratic fit (at least four points, typically several more) but small enough to follow a simple parabolic evolution.
2. A suite of N Monte Carlo realizations is generated by drawing each data point from a Gaussian distribution centered on the photometric data point, and with a standard deviation corresponding to the photometric error bars. In each realization, the boundaries of the region that is fit, particularly after peak where, in most cases, more photometric data points are available, are allowed to oscillate by including or removing up to three data points. The number N of realizations depends on the number of data points N_d used for that particular object: N is the integer nearest to $N_d \log(N_d)^2$, but no smaller than 200:

$$N = \max\left(\mathrm{int}(N_d \log(N_d)^2), 200\right).$$

3. Each realization is fit with a second-degree polynomial. The epochs of maximum brightness and the corresponding magnitudes we report are the mean of the maximum epoch and magnitude distributions in the fit over the family of Monte Carlo realizations and the errors are the corresponding standard deviations.

Figure 5 shows the suite of Monte Carlo realizations generated for SN 2006aj V-band near peak to determine the peak date and magnitude, and their uncertainties. Note that, with a ∼9 day gap in the coverage starting about 4 days after peak, the determination of $\mathrm{JD}_{\mathrm{Vmax}}$ is indeed affected by the choice of boundaries of the region used for the parabola fit. By means of the Monte Carlo simulations, this is reflected in a 0.61 day uncertainty. The Δm_{15} can be estimated as an extrapolation of the polynomial to 15 days. However, we only report this metric when it is sensible to do so: when data cover epochs near 15 days after maximum in the band considered and the quadratic fit is consistent with these data. In the case of SN 2006aj, for example (Figure 5), these criteria are not fulfilled, and the Δm_{15} obtained through polynomial fitting, shown in the figure, is not reported in Table 7.

In Tables 10 and 11 we report the statistical differences we find across our sample in the date of maximum and peak magnitude compared to V. This is helpful to estimate $\mathrm{JD}_{\mathrm{Vmax}}$,

[19] http://www.cosmo.nyu.edu/SNYU
[20] http://www.cfa.harvard.edu/oir/Research/supernova/

Table 7
SN Characteristics (*UBV*)

SN Name	*U* JD (*d*JD)	*U* max (*d*max)	*U* $\Delta m_{15}(d\Delta m_{15})$	*B* JD (*d*JD)	*B* max (*d*max)	*B* $\Delta m_{15}(d\Delta m_{15})$	*V* JD (*d*JD)	*V* max (*d*max)	*V* $\Delta m_{15}(d\Delta m_{15})$
SN 2003jd[a]	...	...	...	52942.50 (0.39)	16.33 (0.05)	...	52942.78 (0.47)	15.93 (0.02)	...
SN 2004aw[b]	...	...	...	53085.55 (0.32)	17.91 (0.03)	0.85 (0.26)	53090.95 (0.85)	17.23 (0.03)	...
SN 2004fe	...	...	...	...	...	...	53318.80 (0.46)	17.09 (0.02)	...
SN 2004gq	53353.86 (2.61)	15.67 (0.09)	...	53353.68 (1.87)	16.12 (0.02)	...	...	...	...
SN 2004gt	...	...	...	53388.52 (1.41)	18.07 (0.05)	...	...	...	...
SN 2005az	...	...	...	...	...	...	53473.36 (0.75)	16.40 (0.05)	0.33 (0.03)
SN 2005bf[c]	53473.20 (0.05)	17.16 (0.03)	...	53474.22 (0.18)	17.66 (0.02)	...	53476.75 (0.42)	17.46 (0.03)	- -
SN 2005bf[c]	53498.54 (0.09)	16.42 (0.02)	1.13 (0.08)	53497.73 (0.14)	16.71 (0.02)	1.12 (0.06)	53498.46 (0.33)	16.43 (0.02)	0.86 (0.02)
SN 2005hg	53679.26 (0.68)	18.25 (0.06)	1.51 (0.45)	53681.51 (0.17)	18.14 (0.02)	1.50 (0.15)	53683.94 (0.27)	17.61 (0.03)	0.93 (0.14)
SN 2005kl	...	...	...	...	...	...	53703.16 (0.56)	16.83 (0.03)	1.07 (0.40)
SN 2005kz	...	...	...	53710.58 (0.76)	19.85 (0.29)	...	53712.44 (0.36)	18.61 (0.05)	0.97 (0.99)
SN 2005mf	...	...	...	...	...	...	53734.06 (0.14)	18.07 (0.02)	0.94 (0.05)
SN 2006T	...	...	...	53780.67 (0.41)	16.81 (0.05)	2.13 (0.10)	53781.56 (0.10)	15.69 (0.02)	...
SN 2006aj	53789.29 (0.78)	17.99 (0.06)	...	53792.68 (0.07)	18.06 (0.03)	...	53794.23 (0.58)	17.51 (0.02)	...
SN 2006el[d]	...	...	...	...	...	...	53984.20 (0.11)	17.57 (0.03)	...
SN 2006ep	...	...	...	53984.96 (0.23)	18.07 (0.05)	1.69 (0.12)	53988.18 (0.08)	17.40 (0.02)	...
SN 2006lv	...	...	...	...	...	...	54045.07 (1.10)	18.44 (0.05)	0.48 (0.19)
SN 2007C	...	...	...	...	...	...	54115.44 (0.51)	16.13 (0.02)	1.05 (0.03)
SN 2007D	...	...	...	...	...	...	54122.81 (0.83)	18.84 (0.13)	1.34 (0.20)
SN 2007ag	...	...	...	...	...	...	54169.76 (0.37)	18.42 (0.03)	...
SN 2007cl	...	...	...	...	...	...	54250.35 (1.00)	17.85 (0.03)	0.64 (0.09)
SN 2007iq	...	...	...	54377.26 (2.97)	19.47 (0.09)	...	...	...	...
SN 2007kj	...	...	...	54378.42 (0.83)	18.14 (0.03)	1.29 (0.29)	54381.96 (0.11)	17.67 (0.02)	1.34 (0.07)
SN 2007ru[e]	...	...	...	...	...	...	54439.95 (0.43)	15.96 (0.01)	0.91 (0.07)
SN 2007rz	...	...	...	54455.49 (1.61)	19.01 (0.17)	...	...	...	...
SN 2007uy	...	...	...	54477.81 (0.10)	16.73 (0.02)	1.30 (0.07)	54481.34 (0.70)	15.76 (0.01)	...
SN 2008D[f]	...	...	...	54491.69 (0.12)	18.42 (0.05)	1.56 (0.09)	54494.24 (0.07)	17.40 (0.02)	0.80 (0.02)
SN 2008bo	...	...	...	54567.80 (0.23)	16.58 (0.02)	2.29 (0.21)	54569.24 (0.16)	16.08 (0.01)	...
SN 2009er	...	...	...	...	...	...	54982.09 (0.16)	17.25 (0.02)	0.90 (0.01)
SN 2009iz	55106.85 (0.38)	18.47 (0.12)		55106.72 (0.17)	17.52 (0.04)	1.08 (0.10)	55108.85 (1.36)	16.97 (0.02)	0.74 (0.09)
SN 2009jf[g]	...	...	...	55119.23 (0.21)	15.66 (0.01)	0.99 (0.05)	55122.32 (0.18)	15.03 (0.02)	0.91 (0.14)

Notes.
[a] Includes data near peak from Valenti et al. (2008).
[b] Includes data near peak from Taubenberger et al. (2006).
[c] Two peaks are visible for SN 2005bf in the *V* band and both are reported here.
[d] Includes data near peak from Drout et al. (2011).
[e] Includes data near peak from Sahu et al. (2009).
[f] Includes data near peak from Modjaz et al. (2009) and Soderberg et al. (2008).
[g] Includes data near peak from Valenti et al. (2011).

which is usually the reference for spectral phases, even in the absence of adequate *V* coverage around the peak.

In Table 2 we report the characteristics of the host galaxies for all objects in our sample. We report the distance to the host galaxy (as heliocentric recession velocity), the absolute and apparent *B* magnitude, when available, and the distance modulus. These quantities are extracted from the HyperLEDA catalog[21] (Paturel et al. 2003). When not available in HyperLEDA, the NASA/IPAC Extragalactic Database catalog is used, and the cosmological parameters used, for consistency with HyperLEDA, are $H_o = 70$ km s^{-1} Mpc^{-1}, $\Omega_m = 0.27$, and $\Omega_\Lambda = 0.73$.

We report the Galactic extinction (E_{B-V}) for each of our objects based on its sky coordinates, and on the most recent dust maps produced by Schlafly & Finkbeiner (2011). Note that these extinction maps deviate by about 10% from the older, commonly used Schlegel et al. (1998) maps in high-extinction regions. The photometry we provided is *not* corrected for Galaxy, host galaxy, cosmological extinction, or reddening.

[21] http://leda.univ-lyon1.fr

Among the supernovae in this sample, over 80% of the objects have spectra collected within our SN program (M14): only SN 2005kz, SN 2006F, SN 2006ba, SN 2006bf, SN 2006cb, SN 2006gi, SN 2006ir, SN 2007aw, SN 2007ke, and SN 2009K do not have any spectral coverage obtained within our group. Spectral information for SN 2007ke exists in the literature, and it indicates that SN 2007ke is an unusual Ca-rich SN Ib (Kasliwal et al. 2011). SN 2008hh does not have spectral coverage within the CfA sample and it only has NIR CfA photometric coverage. Figure 6 shows the epoch of all spectra obtained at FLWO for the objects in our sample. In the bottom portion of the plot, all objects for which the epoch of maximum *V* brightness (JD_{Vmax}) is available are plotted against the bottom *x*-axis: the epoch of the spectra is expressed as days to (since) JD_{Vmax}. In the top portion of the plot, the 17 objects for which we have CfA spectra but JD_{Vmax} is not known (either through our data or in the literature) are plotted against the top *x*-axis, with the epoch expressed as days to (since) our first photometric measurement. Omitted from the plot are all spectra collected at epoch $\gtrsim$90 days, however, our spectroscopic sample contains many nebular phase spectra (M14).

Table 8
SN Characteristics ($RI/r'i'$)

SN Name	$r'(R)$ JD (dJD)	$r'(R)$ max ($d$max)	$r'(R)$ $\Delta m_{15}(d\Delta m_{15})$	$i'(I)$ JD (dJD)	$i'(I)$ max ($d$max)	$i'(I)$ $\Delta m_{15}(d\Delta m_{15})$
SN 2003jd[a]	...	...	...	52945.05 (2.54)	15.61 (0.03)	...
SN 2004aw[a]	53096.04 (0.02)	16.82 (0.03)	0.39 (0.01)	53095.29 (0.80)	16.79 (0.02)	0.57 (0.11)
SN 2004fe	53321.52 (0.68)	17.01 (0.04)	...	53320.09 (0.75)	17.09 (0.03)	...
SN 2004gq	...	...	...	53364.31 (0.24)	15.50 (0.04)	0.25 (0.02)
SN 2005az	53476.10 (0.54)	16.06 (0.03)	...	53479.84 (0.76)	15.97 (0.04)	0.45 (0.05)
SN 2005bf	53499.93 (0.38)	16.36 (0.02)	0.65 (0.05)	53503.58 (0.30)	16.36 (0.02)	...
SN 2005eo	...	...	...	53648.97 (0.63)	18.02 (0.04)	2.57 (1.00)
SN 2005hg	53686.44 (0.40)	17.45 (0.04)	0.64 (0.20)	53688.69 (0.63)	17.33 (0.03)	0.60 (0.14)
SN 2005kl	53704.24 (1.65)	16.07 (0.01)	0.60 (0.23)	53705.12 (0.64)	15.39 (0.02)	0.42 (0.09)
SN 2005kz	...	...	...	53713.18 (1.32)	18.34 (0.06)	...
SN 2005mf	53736.10 (0.47)	17.93 (0.02)	0.78 (0.09)	53737.86 (0.20)	18.16 (0.03)	0.43 (0.09)
SN 2006F	...	...	...	53752.48 (0.58)	17.47 (0.03)	0.57 (0.09)
SN 2006T	53782.52 (0.11)	15.53 (0.03)	1.27 (0.31)	53783.51 (0.38)	15.55 (0.03)	...
SN 2006aj	53794.61 (1.18)	17.44 (0.05)	...	53797.79 (0.14)	17.45 (0.02)	1.08 (0.06)
SN 2006ba	...	...	...	53828.34 (0.73)	17.67 (0.05)	...
SN 2006bf	53827.53 (0.27)	18.71 (0.03)	...	...	...	...
SN 2006cb	...	...	...	53863.53 (0.38)	18.23 (0.04)	...
SN 2006el	53986.00 (0.10)	17.47 (0.02)	...	53987.40 (0.21)	17.45 (0.03)	1.12 (0.21)
SN 2006ep	53990.10 (0.11)	17.23 (0.02)	0.98 (0.06)	53991.58 (0.21)	17.10 (0.02)	0.91 (0.05)
SN 2006fo	54006.61 (0.33)	17.32 (0.02)	0.52 (0.02)	54010.72 (0.54)	17.22 (0.02)	0.43 (0.05)
SN 2006lc	...	...	...	54043.14 (0.13)	17.17 (0.03)	0.71 (0.04)
SN 2007C	54117.80 (0.15)	15.79 (0.01)	...	54119.09 (0.02)	15.56 (0.02)	1.13 (0.04)
SN 2007D	54120.31 (1.91)	18.52 (0.08)	0.67 (0.18)	...	...	...
SN 2007ag	54170.60 (0.31)	18.13 (0.02)	1.07 (0.21)	54171.39 (0.26)	18.04 (0.03)	...
SN 2007ce	...	...	...	54226.61 (0.38)	17.53 (0.02)	0.51 (0.08)
SN 2007cl	54254.09 (0.13)	17.62 (0.02)	0.94 (0.05)	54255.11 (0.14)	17.70 (0.02)	0.82 (0.05)
SN 2007ke	54371.19 (2.68)	18.66 (0.23)	...	...	...	...
SN 2007kj	54383.39 (0.33)	17.56 (0.05)	1.15 (0.26)	54384.23 (0.44)	17.71 (0.06)	0.75 (0.26)
SN 2007ru	54440.64 (0.32)	15.87 (0.02)	0.68 (0.03)	54442.68 (0.40)	15.78 (0.02)	0.72 (0.04)
SN 2007rz	54455.74 (1.94)	18.23 (0.26)	...	...	...	...
SN 2007uy	54484.75 (0.24)	15.56 (0.02)	0.95 (0.06)	54485.64 (0.68)	15.59 (0.02)	...
SN 2008D	54495.47 (0.11)	16.99 (0.02)	0.89 (0.03)	54497.19 (0.45)	16.65 (0.02)	0.57 (0.12)
SN 2008aq	54530.28 (3.20)	15.85 (0.07)	0.40 (0.22)	54536.92 (0.68)	16.04 (0.05)	...
SN 2008bo	54570.33 (0.59)	16.02 (0.02)	1.20 (0.28)	54571.11 (0.30)	16.08 (0.03)	1.04 (0.22)
SN 2009er	54984.00 (0.24)	17.19 (0.02)	1.00 (0.29)	54985.08 (0.49)	17.26 (0.02)	0.47 (0.04)
SN 2009iz	55111.73 (0.25)	16.84 (0.02)	0.65 (0.04)	55115.67 (0.23)	16.82 (0.02)	0.45 (0.03)
SN 2009jf	55123.52 (0.07)	15.00 (0.01)	0.52 (0.04)	55124.92 (0.10)	15.01 (0.02)	0.43 (0.03)

Note. [a] Photometry collected with Johnson R and I filters.

Table 9
SN Characteristics (JHK_s)

SN Name	J JD (dJD)	J max ($d$max)	J $\Delta m_{15}(d\Delta m_{15})$	H JD (dJD)	H max ($d$max)	H $\Delta m_{15}(d\Delta m_{15})$	K_s JD (dJD)	K_s max ($d$max)	K_s $\Delta m_{15}(d\Delta m_{15})$
SN 2004gk	53458.33 (2.49)	16.39 (0.12)	...	...	...	...	...	...	...
SN 2004gt	...	...	...	...	...	...	53472.00 (0.45)	15.63 (0.28)	...
SN 2005bf	53505.32 (0.44)	15.90 (0.01)	0.39 (0.02)	53511.45 (2.03)	15.81 (0.07)	0.18 (0.11)	53512.49 (1.69)	15.57 (0.03)	0.26 (0.04)
SN 2005eo	...	...	...	...	...	...	53659.95 (1.62)	15.57 (0.09)	0.40 (0.13)
SN 2005hg	53692.40 (0.61)	16.54 (0.03)	0.53 (0.07)	53693.73 (0.44)	16.55 (0.06)	0.29 (0.03)	53695.95 (0.70)	16.37 (0.08)	0.44 (0.08)
SN 2005kl	53706.57 (1.20)	13.78 (0.04)	0.28 (0.04)	53713.94 (1.70)	13.34 (0.12)	0.50 (0.09)	53706.71 (3.34)	12.97 (0.09)	0.22 (0.05)
SN 2005mf	53740.91 (0.41)	17.41 (0.03)	0.61 (0.17)	53742.27 (0.27)	17.27 (0.05)	0.97 (0.25)	53743.06 (0.38)	16.93 (0.09)	0.80 (0.12)
SN 2006aj	53793.79 (2.09)	16.95 (0.12)	...	53793.85 (1.62)	16.70 (0.13)	...	53793.11 (0.76)	16.39 (0.11)	...
SN 2006fo	54020.38 (0.62)	16.26 (0.09)	0.49 (0.07)	54018.35 (3.42)	16.39 (0.16)	0.14 (0.05)	54018.04 (0.99)	17.03 (0.15)	0.51 (0.12)
SN 2007ce	54231.00 (2.65)	17.26 (0.16)	0.35 (0.29)	54237.21 (1.77)	17.51 (0.22)	...	...	...	...
SN 2007uy	54490.08 (0.09)	14.79 (0.02)	0.48 (0.03)	54491.36 (0.19)	14.62 (0.03)	0.47 (0.03)	54492.40 (0.11)	14.35 (0.03)	0.47 (0.03)
SN 2009er	54990.32 (0.28)	16.60 (0.02)	0.99 (0.14)	54989.98 (1.05)	16.64 (0.13)	0.63 (0.14)	...	...	...
SN 2009iz	55120.83 (0.14)	16.24 (0.01)	0.33 (0.01)	55125.04 (0.38)	16.24 (0.03)	0.23 (0.02)	55123.23 (0.34)	15.73 (0.18)	0.23 (0.02)
SN 2009jf	55129.12 (0.15)	14.42 (0.03)	0.23 (0.02)	55130.40 (0.33)	14.29 (0.06)	0.36 (0.13)	55133.06 (0.25)	13.89 (0.03)	0.54 (0.04)

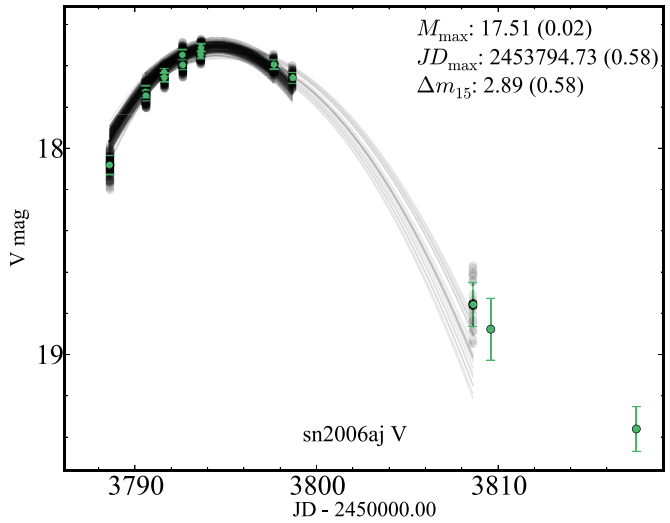

Figure 5. Suite of Monte Carlo realizations generated for SN 2006aj *V*-band near peak to determine the peak date and magnitude and associated uncertainties. In each realization, a subset of data points is selected where one, two, or three data points at the edges of the set may or may not be included. A synthetic photometric data set is then generated by drawing a data point (gray circle) for each epoch within a Gaussian distribution centered on the photometric datum (green circle) and with standard deviation equal to its error bar. The synthetic photometry is fit with a parabola (gray line). The date of peak, the magnitude at peak, the Δm_{15} reported, and their related uncertainties are calculated as the mean and standard deviation of the corresponding values across all realizations.

(A color version of this figure is available in the online journal.)

5. COMPARISON WITH LITERATURE DATA

Out of the 64 objects that comprise our sample, 37 objects have published photometry. The objects for which data are available in the literature are marked in Table 1. When photometric measurements exist for an object in the same photometric system as our monitoring program or the photometric conversion is trivial (when the photometric system for the data available in the literature is well defined) we compare our data with the published photometry. In addition, when more data around maximum are available, our data are combined with the literature data to derive a more accurate date of maximum in *V*, following the procedure described in Section 4 and Figure 5.

We find that our photometry is generally consistent within the errors with published photometry for the objects in our sample (Figure 7), with one notable exception: D11 offered the most complete study of stripped SN light curves to date, and our samples share 17 stripped SNe. D11 published photometry in *V* and *R*. When compared with our photometry, only two objects appear to be in excellent agreement in both bands: SN 2004gk and SN 2006jc. SN 2005hg and SN 2007C agree well in *V*, but show an offset in *R*. In addition, for SN 2005la and SN 2006jc, an independent confirmation of the magnitude is also available. The D11 photometry of SN 2006jc includes data from Foley et al. (2007) and Pastorello et al. (2007), and the photometry agrees well with ours. The D11 photometry of SN 2005la includes measurements from Pastorello et al. (2008a), and although the light curves from both the D11 survey and our survey are noisy, they are in reasonable agreement.

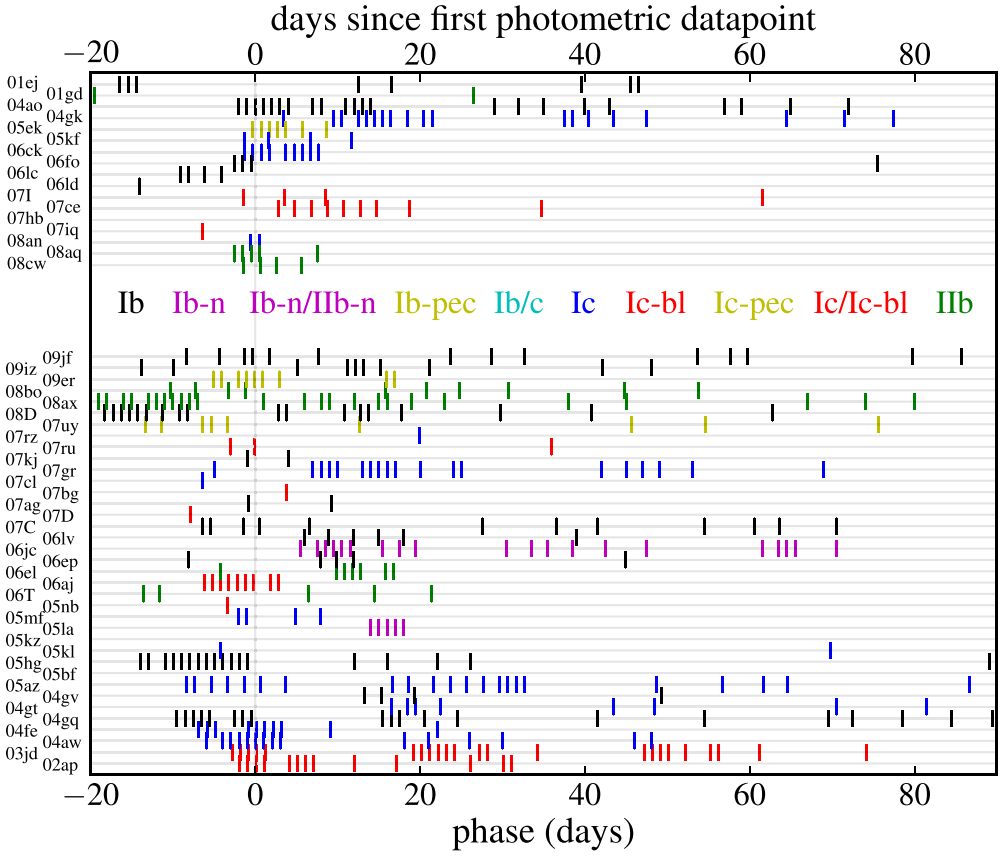

Figure 6. Phases of spectroscopic observations for all SNe in our sample for which CfA FLWO 1.5 m FAST spectra are available as published in M14. The SN classification is indicated by the color of the marks as defined by the inset list. For the top set of 17 SNe the JD_{Vmax} is not known and thus the phases of the spectra are defined as days since our first photometric measurement. The phases for the bottom set of 37 SNe are plotted with respect to the JD_{Vmax} calculated as in Section 4.

(A color version of this figure is available in the online journal.)

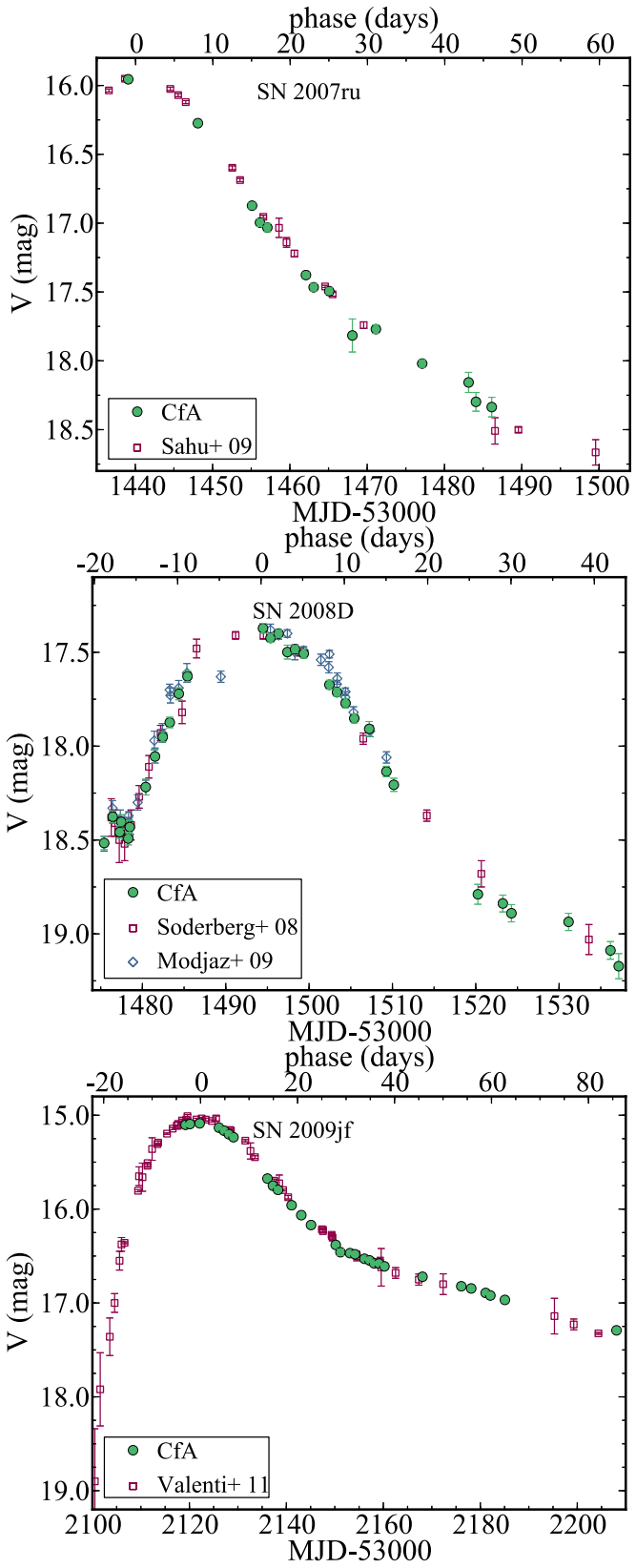

Figure 7. CfA stripped SN *V*-band light curves compared with *V*-band light curves from the literature. Top: SN 2007ru, with data from Sahu et al. (2009), middle: SN 2008D, including data from Soderberg et al. (2008) and KAIT data from Modjaz et al. (2009), and bottom: SN 2009jf with data from Valenti et al. (2011). Our photometry agrees with the literature photometry for these objects within the quoted errors. We have shown only *V*-band data here for clarity, but the photometry is similarly consistent in other bands.

(A color version of this figure is available in the online journal.)

Table 10
Peak Epoch by Band[a]

Band	Weighted Average	Median	Standard Deviation
U	−1.2	−3.3	2.1
B	−2.3	−2.3	1.3
R/r'	1.8	1.5	1.3
I/i'	3.5	3.1	1.5
J	8.5	6.9	3.3
H	10.1	9.8	4.3
K	10.5	10.9	5.0

Notes. [a] Difference in days between *V* maximum epoch JD_{Vmax} and peak epoch in each band. Negative values indicate the peak happens before JD_{Vmax}.

Table 11
Magnitude at Maximum Brightness Compared to V_{max}

Band	Weighted Average	Median	Standard Deviation
U	−0.13	−0.20	0.27
B	−0.70	−0.62	0.16
R/r'	0.21	0.19	0.16
I/i'	0.25	0.17	0.32
J	0.91	0.73	0.71
H	1.04	0.81	0.81
K	1.35	1.19	0.87

For the remaining objects, where the coverage overlaps, allowing a comparison, we note that the D11 photometry is brighter, with up to a magnitude difference in *R* at peak and over 0.5 mag in *V* (e.g., SN 2006fo, Figure 8). The discrepancy typically increases as the SNe evolve, growing as large as ∼1.5 in *V* and ∼2 mag in *R* at later epochs (≳50 days, e.g., SN 2007D, SN 2006fo). Figure 9 shows the evolution of the mean discrepancy in the *V* band between the D11 and CfA surveys as a function of phase. Photometric measurements are included if the separation in time between the D11 and CfA photometry is less than 5 days for epochs earlier than 45 days after JD_{Vmax}, and less than 10 days for later epochs. A single SN can contribute to each bin with one or more data points. Error bars represent the error in the mean offset for each epoch (standard deviation over square root of the number of data points that generates the mean). The mean evolution is shown for all objects as well as after excluding SN 2005la and SN 2006jc.

Figure 10 shows a histogram of the distribution of *V*-band magnitude offsets for data points within 5 days of JD_{Vmax}, within 5 days of phase = 40 days after JD_{Vmax}, and for any epoch later than 45 days after JD_{Vmax}. Note that all offsets are positive or zero at best, indicating that the D11 photometry is always brighter than the CfA photometry, and at later epochs, the discrepancy increases as the D11 light curves reach a plateau.

For all of these objects, our measurements are generated as PSF fitting photometry on host-subtracted images, while D11 performed PSF fitting photometry on the original images without host subtraction. Thus, we attribute this discrepancy to galaxy contamination in the D11 sample. The discrepancy is consistent with the well-known effect of host-galaxy contamination on SN light curves, as the SN fades and becomes less bright in comparison to the host galaxy, as described in Boisseau & Wheeler (1991). Additionally, our photometry has proven to be consistent at the level of a few hundredths of a magnitude on average for a large sample of SN Ia (Hicken et al. 2012, 2009). Visual inspection of the SN images shows that several objects for which the difference is largest are in fact close to the core

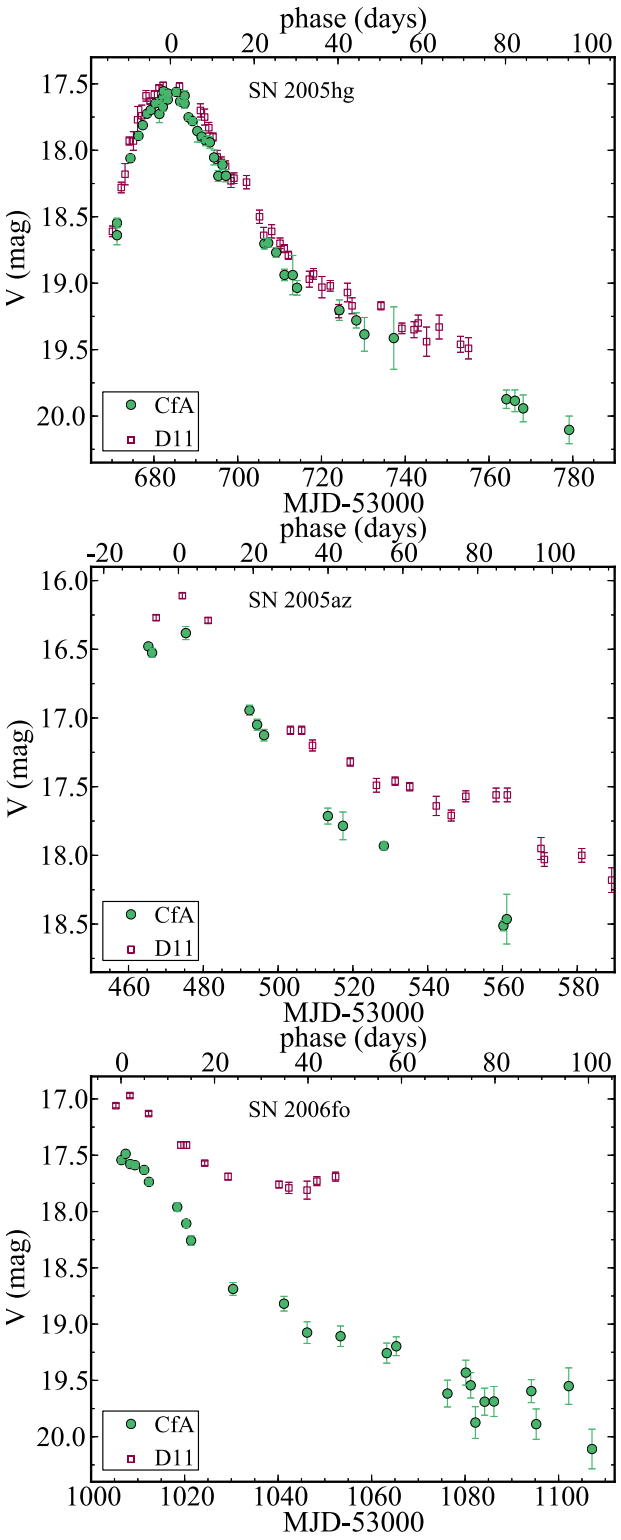

Figure 8. *V*-band light curves from our survey and D11 for SN 2005hg (top), SN 2005az (middle), and SN 2006fo (bottom), respectively, from the "gold," "silver," and "bronze" D11 subsamples (see the text). SN 2005hg shows excellent agreement in *V* (although an offset is present in *R*), while both SN 2005az and SN 2006fo show a significant photometric offset, with D11 brighter at all epochs, a behavior observed in the majority of the objects in common between the two samples. The discrepancy grows at later epochs when the SN is fainter, which is consistent with the D11 photometry being brighter due to host-galaxy contamination in the photometric measurements. Only *V*-band data are shown, as the *V* standardized magnitudes are reported by both surveys in the same photometric system, but similar discrepancies are seen in *R* after photometric transformations are applied.

(A color version of this figure is available in the online journal.)

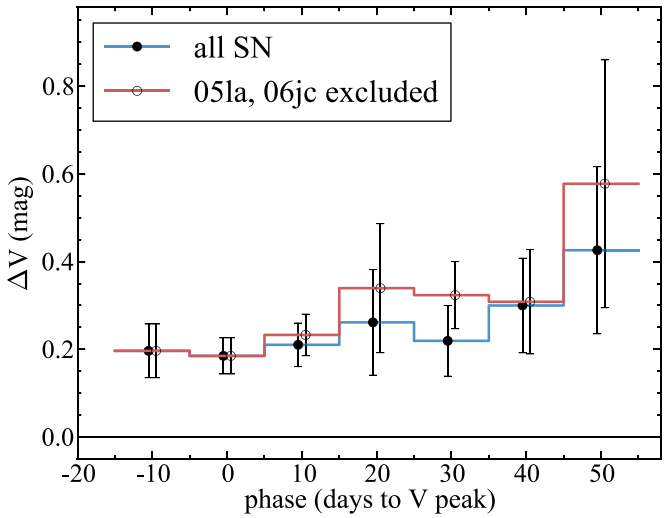

Figure 9. *V* magnitude difference between D11 and our (CfA) data ($\Delta V = V_{\rm CfA} - V_{\rm D11}$). For each light curve, the data with the closest dates of observations between the surveys are used, and data are only included when the observations are separated by less than 5 days (10 days for epochs later than 45 days to peak). Error bars represent the error in the mean offset for each epoch ($\sigma/\sqrt{N}$). The blue line (filled circles) includes all objects in common, while red line data (empty circles) exclude SN 2005la and SN 2006jc (see the text). The offset is minimum near peak magnitude and increases as the SNe get dimmer. Note that all values are positive, indicating that the D11 photometry is consistently and significantly brighter than our photometry at all epochs.

(A color version of this figure is available in the online journal.)

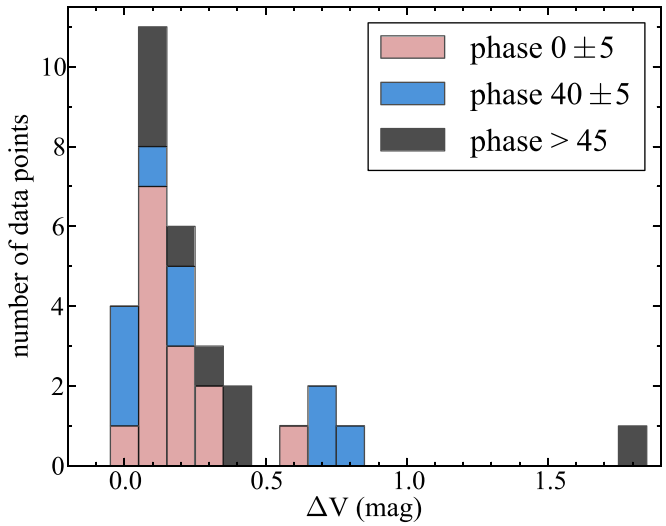

Figure 10. Distribution of the photometric discrepancy between the D11 data and our data (see Figure 9) shown as a stacked histogram. Different colors represent different epochs (blue: 0 ± 5 days; red: 40 ± 5 days; black: >45 days). All values are positive, indicating that the D11 photometry is consistently brighter than our photometry. The difference between D11 and our data is more prominently skewed toward high ΔV at late epochs than near peak. The D11 light curves plateau at these late phases, an effect which we attribute to residual galaxy contamination in the D11 photometric analysis.

(A color version of this figure is available in the online journal.)

of the host galaxy (e.g., SN 2006fo) or in bright regions of the host-galaxy arms (e.g., SN 2004gt, SN 2004fe).

D11 classified their sample by quality into three groups: a gold, a silver, and a bronze subset. The latter is judged too poor to be used for the analysis and all inference in D11 is based on the gold and silver objects. We note that, although still typically brighter than our measurements, the data in the gold

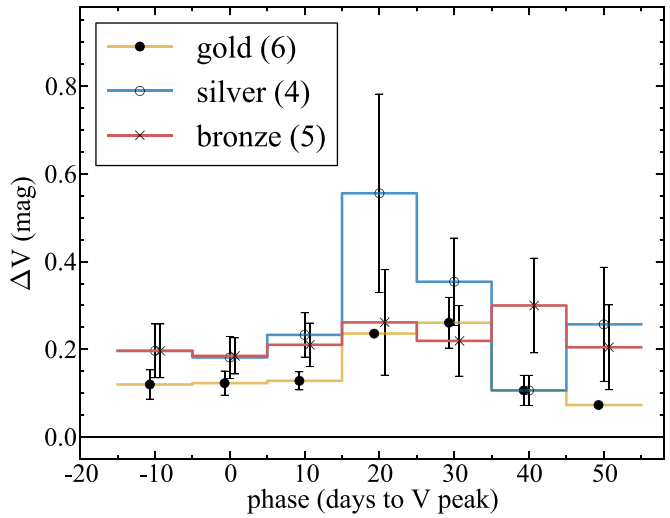

Figure 11. V magnitude difference between D11 and our (CfA) data averaged in 10 day bins of phase, as in Figure 9. The D11 data are shown separately for each of the different quality samples in the D11 paper. These samples were ranked from best to worst as "gold" (yellow line, solid circles), "silver" (blue line, empty circles), and "bronze" (red line, X's). The number of objects in each subsample is shown in parenthesis. D11 used only their gold and silver samples in their analysis.

(A color version of this figure is available in the online journal.)

sample are in best agreement with our data, while the silver and bronze samples show the largest offsets (see Figures 8 and 11). The host contamination in the D11 sample may affect the time evolution of the SNe, and particularly the Δm_{15} estimates, and the use of the $V-R$ color evolution in correcting the host-galaxy extinction, since, in addition to giving rise to an offset in magnitude, the contamination is worse at later epochs and is different in different bands.

Finally, in addition to the 17 stripped SNe common to our samples, D11 presents photometry or SN 2005eo, which was also monitored at the CfA. SN 2005eo is included in the D11 silver sample, and was originally classified as a SN Ic. SN 2005eo was, however, removed from our stripped SNe sample, as we reclassified this object as a SN Ia (M14). This classification is further discussed in Section 7.3.4.

6. COLORS AND COLOR EVOLUTION

Our multi-wavelength photometric coverage allows us to discuss the color characteristics and color evolution of the supernovae in our sample. While an in-depth discussion is beyond the scope of this paper, and it will be presented in (F. B. Bianco et al., in preparation); here we present the basic color evolution and color–color behavior of our stripped SNe sample.

When we discuss colors, color evolution, and for all plots in color space, we correct the magnitude of all objects in our sample for Galactic extinction only. The Galactic extinction E_{B-V} is obtained by adopting the Schlafly & Finkbeiner (2011) recalibration of the Schlegel et al. (1998) extinction maps, with the E_{B-V} reported in Table 2. For each photometric band, we use the extinction coefficients A_λ normalized to the photoelectric measurements of E_{B-V} as reported in Table 6 of Schlegel et al. (1998), which assume a reddening law according to Fitzpatrick (1999) with $R_V = 3.1$, and standard transmission for the Landolt $UBVRI$, the SDSS $r'i'$, and 2MASS JHK_s filters. These extinction corrections are based on star spectra and we do not correct the extinction for the SN spectral energy distribution (SED). Based on Jha et al. (2007), who studied this effect for SNe Ia, we estimate the correction on R_V to be $\lesssim$4%. No host reddening or cosmological corrections are applied. While with spectra and NIR data, the host reddening can be constrained (F. B. Bianco et al., in preparation), here we use the observed color. This approach is sensible to aid the photometric differentiation of subtypes.

Figure 12 shows color–color plots for our sample of stripped SNe in $B-V$ versus $r'-i'$, $B-V$ versus $V-H$, and $r'-i'$ versus $V-H$ space. The error bars in the plot are generated by adding photometric errors in each band in quadrature (disregarding correlation). All objects with a solid determination of $\mathrm{JD_{Vmax}}$, either in the literature or derived from our data (Section 5), are included in these plots when photometry data are available within eight days of $\mathrm{JD_{Vmax}}$ for all four bands used in each plot. In $B-V$ versus $r'-i'$ this amounts to 47 objects: 8 SNe IIb, 15 Ib, 13 Ic, and 6 Ic-BL. Identified as "other" are objects for which we could not determine a subtype (SN 2007iq, which is of uncertain classification, Ic or Ic-BL, as only late spectra are available), or that appear spectroscopically atypical (the Ca-rich transient SN 2007ke, the narrow-line SN 2005la, and the SN Ib-pec 2007uy and SN 2009er). The spectroscopic characteristics of these objects are discussed in detail in M14 and the photometric properties of SN 2007ke and SN 2005la are discussed in Section 7. The ellipses in the plot represent the mean (center) and standard deviation (σ) of each subtype distribution.

In $B-V$ versus $r'-i'$, all distributions are consistent with each other to the 1σ level: the subtypes cluster in overlapping distributions and appear indistinguishable in this color–color space (Figure 12, top panel). When NIR colors are used, the subtypes seem to separate in color–color space, although the number of objects available for this analysis is smaller. When including NIR colors ($V-H$), the number of objects that can be used for this plot drops significantly, as only 15 objects in our sample have a determination of $\mathrm{JD_{Vmax}}$ *and* optical and NIR photometry within eight days of it. These objects include eight SNe Ib, two SNe Ic, and two SNe Ic-BL, and the peculiar objects SN 2007uy and SN 2009er (in these plots under the label "other"). Subtypes separate to $\gtrsim 1\sigma$ level, particularly in $r'-i'$ versus $V-H$. The $V-H$ distribution in fact shows the broadest variation, while the $r'-i'$ is the narrowest. Among the SNe IIb only SN 2008ax has NIR coverage, but unfortunately, there is no optical coverage from FLWO for this SN, thus no SNe IIb were included in the $B-V$ versus $V-H$ or $r'-i'$ versus $V-H$ plot. The mean of the distribution of SNe Ib and Ic is still consistent within 2σ, but SNe Ib appear redder in $V-H$, and SNe Ic-BL bluer, though this observation is based on only two SNe Ic-BL and it needs to be verified in larger samples.

While these trends are based on small samples, they highlight the importance of NIR photometry, and we suggest populating such $r'-i'$ versus $V-H$ color–color plots in the future to verify the SN-type-dependent color trends observed here, which ultimately could be used to differentiate core–collapse SN subtypes photometrically.

We plot the color evolution of our objects in $B-V$, $r'-i'$, and $V-H$ in Figure 13. In each plot, all photometric data between -20 and 210 days with respect to the epoch of peak V magnitude, $\mathrm{JD_{Vmax}}$, are plotted in the bottom panel for all SNe with well-determined $\mathrm{JD_{Vmax}}$. *All* objects in our sample with known $\mathrm{JD_{Vmax}}$ are on display here. The error bars represent the photometric errors. The scatter in the bottom panels of this

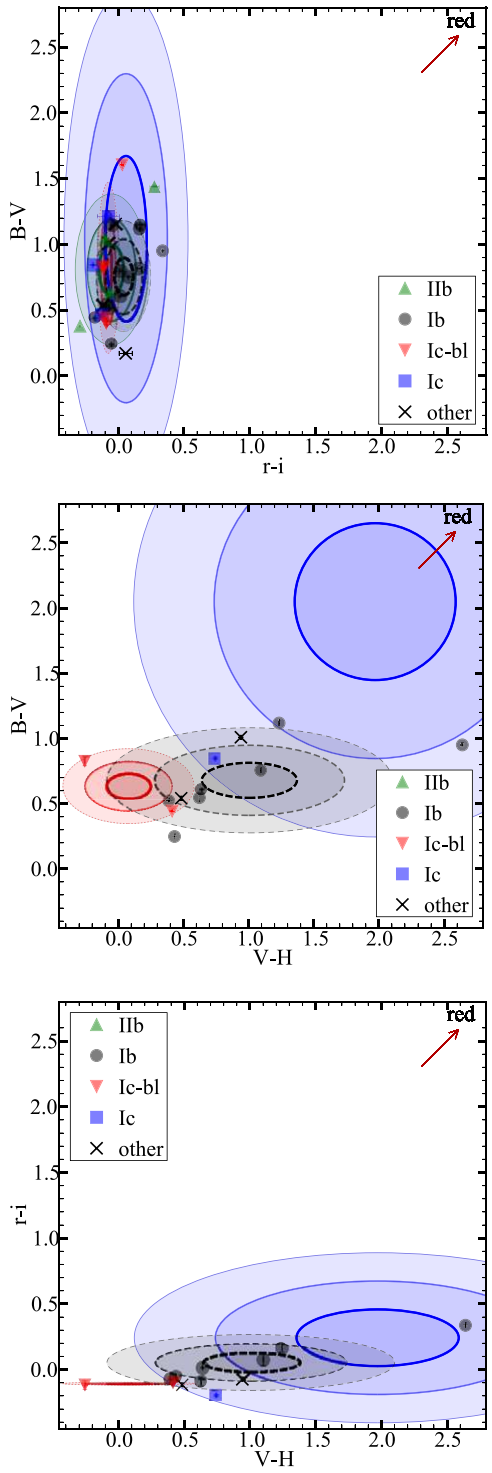

Figure 12. Color–color distributions at JD_{Vmax} for the SNe presented in this paper: (top) $B-V$ vs. $r'-i'$; (middle) $B-V$ vs. $V-H$; (bottom) $r'-i'$ vs. $V-H$. Different SN types are indicated by different symbols: IIb = green triangles, Ib = gray circles, Ic = blue squares, Ic-BL = red upside-down triangles; other subtypes are indicated by X's. Ellipses (same color mapping by subtype) are centered on the mean of each subtype distribution with their semi-major and semi-minor axes given by the 1, 2, and 3σ projected single-color distributions. The large standard deviation of the Ic sample (shown in blue) is dominated by the contributions of the very red SN 2005kl which is outside the plotted range at $B-V = 3.25 \pm 0.08$ mag, $r-i = 0.6734 \pm 4 \times 10^{-4}$ mag, and $V-H = 3.21 \pm 0.05$ mag. All colors are the closest available to JD_{Vmax} and only included if the epoch in both bands is within five days of JD_{Vmax} epoch. The arrow simply indicates the direction of redder colors (i.e., a reddening vector with $A = 1$).

(A color version of this figure is available in the online journal.)

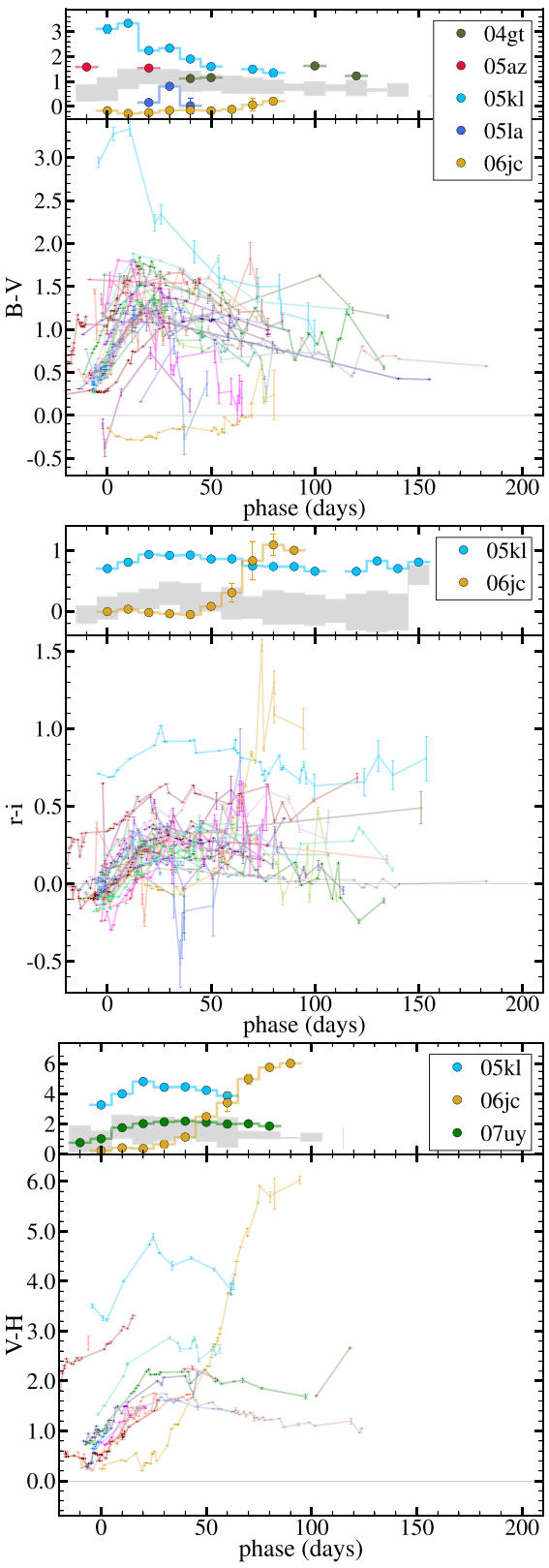

Figure 13. Color evolution of the objects in our sample with determined JD_{Vmax}: (top) $B-V$, (middle) $r-i$, and (bottom) $V-H$. For each color plot, the bottom panel shows the color evolution of all objects along with their photometric errors. The top panel shows the 1σ weighted average color evolution range (gray region) for objects with defined colors at JD_{Vmax}. Outliers are illustrated and named separately in these top panels with their color curves binned in 10 day intervals.

(A color version of this figure is available in the online journal.)

plot thus represents the diversity in the observed photometry of stripped SNe.

The top panel shows the mean color evolution, binned in 10 day intervals, and its standard deviation as a gray area. This is the weighted average of the photometry for all objects calculated over 10 day bins, weighted by the photometric errors. The standard deviation in the average is calculated as the second moment of the distribution of photometric measurements, disregarding the photometric errors. The weighted average colors for a more complete set of color spaces are shown in Figure 14. Outliers are plotted in color in Figure 13 in each top panel, with the same 10 day binning and error bars representing the standard deviation within the bin. All objects with a binned color data point with a 2σ lower (upper) limit above (below) the average by more than two standard deviations (standard deviations of the average in this case) are considered outliers, are plotted in this panel, and are identified in the legend. Note that SN 2006jc (Section 7.3.2) is an obvious outlier in each of these plots (gray circles) with early blue and late red colors. SN 2006jc is removed from the calculation of the mean color evolution, as it is known to be spectroscopically peculiar and its late-time color-evolution is driven by non-intrinsic SN processes such as dust formation (see Section 7.3.2 and references therein). Other outliers are discussed in Section 7.

Finally, we present the average color evolution across our sample and its standard deviation, in Figure 14 for $B-V$, $r'-i'$, and $V-H$ (left), and $U-B$, $V-r'$, $H-J$, and $J-K$ (right). For $B-V$, $r'-i'$, and $V-H$, these averages also appear as shaded regions in Figure 13. The average, weighted by the photometric errors, is generated in each color band as described in the previous paragraph, again excluding SN 2006jc.

We notice the following.

1. The largest color variation is observed in $V-H$: in time, (Figure 14), as well as among different SN types (as already noted in Section 6 and Figure 12, and indicated by the large standard deviation in this plot). Two causes may contribute to this effect: the small size of the sample that has photometry near JD_{Vmax} in both V and H, which is only 20 objects, and host-galaxy reddening effects. High reddening would have the most impact on the bluest and the least on the reddest band, and would result in a large effect in $V-H$, since we are bridging an interval of over 1100 nm in wavelength. However, reddening would affect the spread in color equally at all epochs (the standard deviation of the mean color, which is large, typically $\sim$1.5 mag). The color *evolution* over time is due to intrinsic changes in the SN SED as the SN evolves. The mean $V-H$ color spans a dramatic 1.6 mag between 10 days before and 50 days after peak.
2. The least variation is in $r'-i'$: only 0.5 mag total as seen in Figure 14 both for the standard deviation and for the change in mean color over time. Narrow standard deviations are also observed in $H-J$ and $V-r'$, while $J-K_s$ shows remarkably little color evolution.
3. The $r'-i'$ colors at peak are intriguingly similar for all objects. This was also noticeable in Figure 12, especially for SNe Ic-BL, although only six and two SNe Ic-BL are plotted, respectively, in the top panels and two bottom panels due to the availability of photometry in all four bands needed for each plot. However, we can measure the $r'-i'$ color within 10 days of JD_{Vmax} for seven SNe Ic-BL. We find a mean $r'-i'$ peak color for SNe Ic-BL of $< r'-i' >_{peak} = -0.025 \pm 0.01$ mag. The standard deviation for the distribution of other types is at least twice as large.

These color evolutions and the relation between colors are worth a more thorough investigation since they will be valuable in typing and classification in synoptic surveys where the data volume renders spectroscopic identification infeasible, and follow-up resources will be scarce compared to the number of discoveries. A more complete analysis of the colors of stripped SNe and their correlations with types will be presented in F. B. Bianco et al. (2014, in preparation) including SN data from the literature.

7. DISCUSSION OF SPECIFIC SUPERNOVAE

7.1. SN 2005bf

Some CfA optical and NIR photometric measurements of SN 2005bf were published in Tominaga et al. (2005), but the data presented here used template subtraction and more comparison stars for the reduction and they supersede the measurements in Tominaga et al. (2005). SN 2005bf was an unusual SN Ib with unique photometric and spectroscopic properties (Mattila et al. 2008; Tominaga et al. 2005; Folatelli et al. 2006; Maeda et al. 2007; Maund et al. 2007), interpreted as a strongly aspherical explosion of a Wolf–Rayet WN star, perhaps with a unipolar jet (Tominaga et al. 2005; Folatelli et al. 2006; Maund et al. 2007) and possibly powered by a magnetar at late times (Maeda et al. 2007).

Our light curve has excellent multi-band coverage of the region around peak brightness, both before and after peak: the first CfA optical epochs were collected on JD 2553471.742 (U), while NIR coverage began 10 days later. The CfA optical and NIR light curve of SN 2005bf is shown in Figure 15, left panel. An early peak is clearly identifiable in the bluer bands U and B, and (less clearly) in V on JD2453476.75. A later, more prominent peak, visible in all bands, occurs in V on JD 2453498.96 (JD_{Vmax}). Our photometric coverage continues through JD 2553526 in optical wavelengths and JD 2553525 in NIR. An in-depth phenomenological discussion of these peaks was presented in Tominaga et al. (2005), and Folatelli et al. (2006). We note that the first peak is too late after explosion to be consistent with a standard shock breakout (as seen in SN 2008D; Soderberg et al. 2008; Modjaz et al. 2009), while if the second peak is considered, the rise time for this SN is unusually long (over 30 days!). The second maximum and long rise time has been attributed to the highly aspherical distribution of a large amount of ^{56}Ni synthesized in the explosion (Tominaga et al. 2005; Folatelli et al. 2006). M14 discuss how the choice of the epoch for the peak affects the spectroscopic analysis of SN 2005bf.

7.2. SN 2007ke

SN 2007ke is a known Ca-rich transient with seven photometric data points in KAIT R published in Kasliwal et al. (2011). Our data do not cover the rise of the light curve; thus, we estimated the V-band maximum using the Kasliwal et al. (2011) data according to the prescription described in Section 4, and applying a shift corresponding to the median difference in time between R and V reported in Table 10. Adding the error to the fit (0.32 days) and the standard deviation in the time offset (1.4 days, Table 10) in quadrature, we obtain $JD_{Vmax} = 2454371.2 \pm 2.1$. While our photometry is sparse and our coverage begins near peak,

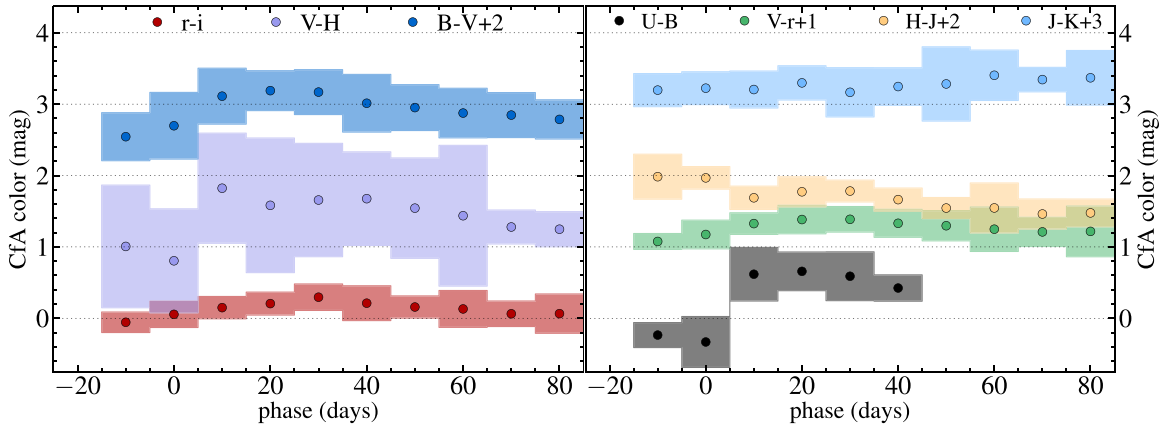

Figure 14. Average color evolution of the stripped SNe in our sample in several color bands. The weighted average, weighted by the photometric errors, is generated in each color band, excluding SN 2006jc. Colors are calculated from our photometry, then binned in 10 day intervals. The sample standard deviation is visualized as a shaded region. The SNe are corrected for galactic reddening, but not for host extinction. We have eight and five data points for $V-H$ at phases 70 and 80 days, respectively, and six for $U-B$ at both the 30 and 40 day phases. All other bins include 10 or more data points. Epochs later than 40 days are omitted for $U-B$ as $\lesssim$3 data points are available. These weighted averages for $B-V$, $r-i$, and $V-H$ are also shown in the top panels of figure Figure 13.

(A color version of this figure is available in the online journal.)

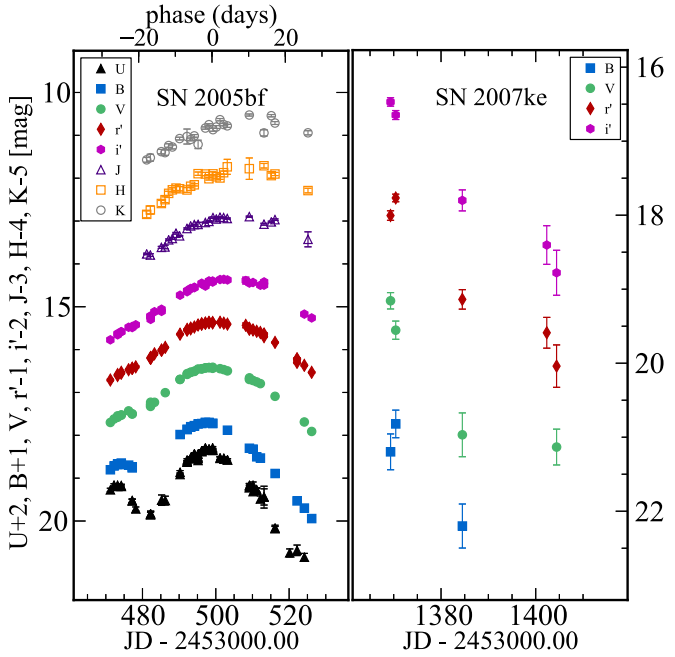

Figure 15. Optical and NIR photometry of SN 2005bf (left) and SN 2007ke (right); symbols as described in Figure 2.

(A color version of this figure is available in the online journal.)

we have coverage in four bands, $BVr'i'$, with four epochs in B and V, including a non-detection at JD = 2454402.8, and five in $r'i'$. This allows us to probe color evolution, and we notice that SN 2007ke shows scatter (Figure 15, right panel). Additionally, it was noted (Kasliwal et al. 2011) that SN 2007ke is well removed from its host galaxy (compare its separation of $\sim$0.″5 from the center of the host, Table 2, with NGC 1129's radius of 1.″6: the extinction-corrected apparent semi-major axis of the 25 B magarcsec^{-2} isophote reported by HyperLEDA; Paturel et al. 1991). Additionally, SN 2007ke is the only SN in our sample to arise in an elliptical host galaxy (see Table 2), confirming that the environments of Ca-rich transients are unusual compared to stripped SN host environments, as pointed out in Kasliwal et al. (2011).

7.3. Unusual Color Evolution

Figure 13 shows the color evolution of our SNe in $B-V$, $r'-i'$, and $V-H$. The top panel in each of the three plots shows the mean color evolution, as described in Figure 14, and overplotted are the color curves for outliers: objects whose color, binned in 10 day intervals, is at least 2σ away from the 2σ limit of the color average in one or more bins. Three obvious outliers in these plots are discussed in this section: SN 2006jc, SN 2005kl (both outliers in all three color spaces), and SN 2005la (an outlier in $B-V$, and for which we have no NIR coverage). Additionally, SN 2008D is a $>2\sigma$ outlier in both $r'-i'$ and $V-H$. Although SN 2004gt, SN 2005az, and SN 2007uy, also appear in the top plots in Figure 13 as outliers in one color space, their classification as outliers is weak due only to the distance of one early (SN 2005az) or one late 10 day bin (SN 2004gt, SN 2007uy) from the sample average, and they are not discussed individually.

7.3.1. SN 2008D

SN 2008D is a well-studied SN Ib (Soderberg et al. 2008; Mazzali et al. 2008; Modjaz et al. 2009; Malesani et al. 2009), discovered in the X-ray while *Swift* monitored the host galaxy to observe the evolution of SN 2007uy (Soderberg et al. 2008), thus yielding very stringent optical and NIR pre-explosion limits only hours before explosion (Modjaz et al. 2009). Our data on SN 2008D were already published in Modjaz et al. (2009), and they are presented again here for completeness. SN 2008D does not appear as an outlier in Figure 13, but it is a $>2\sigma$ outlier in both $r'-i'$ and $V-H$ colors. Its light curve is redder than the mean over the entire evolution, and in fact, SN 2008D is known to suffer significant host reddening ($A_v \sim$ 1.5–2.5 mag, Soderberg et al. 2008) in addition to the early (prior to $-$10 days to JD_{Vmax}) blue excess attributed to cooling of the shock-heated stellar envelope (Modjaz et al. 2009).

7.3.2. SN 2006jc

SN 2006jc is classified as a SN Ib-n. A re-brightening in the NIR light curve of SN 2006jc was first noted by Arkharov et al. (2006). Our NIR data have exquisite sampling of the NIR re-brightening, which begins near JD 24541050, or roughly 40 days

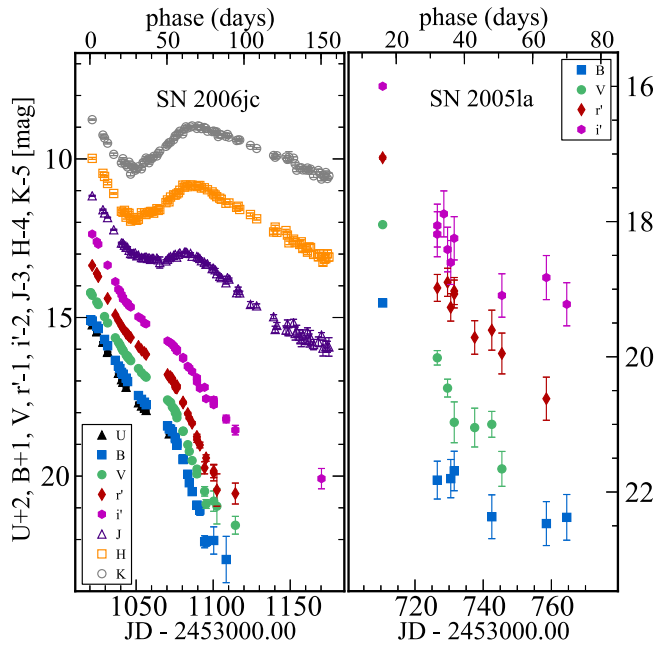

Figure 16. Optical and NIR photometry of SN 2006jc (left) and SN 2005la (right); symbols are the same as described in Figure 2.

(A color version of this figure is available in the online journal.)

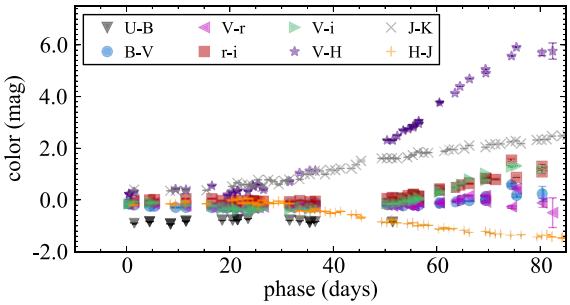

Figure 17. Color time series for SN 2006jc. The error bars are the quadrature sum of the photometric errors for the constituent bands.

(A color version of this figure is available in the online journal.)

after peak, adopting the peak determination of Pastorello et al. (2008a) and continues with regular sampling through ∼160 days after peak. We also present regular photometry in optical bands that continues through 100 days after peak. Optical and NIR photometry of SN 2006jc can be found in the literature (Mattila et al. 2008; Pastorello et al. 2008a). We plot our light curve in Figure 16 (left panel) and color time series in Figure 17. The unusually blue early color of SN 2006jc at early times and its later NIR re-brightening have been explained by complex interaction with circumstellar material. The early blue color is due to interaction with He-rich material ejected by the progenitor in prior outbursts (Pastorello et al. 2007; Foley et al. 2007; Smith et al. 2008), and the reddening is due to production of dust triggered in the ejecta at later epochs (Mattila et al. 2008; Pastorello et al. 2008a).

7.3.3. SN 2005la

SN 2005la (Figure 16, right panel) is spectroscopically peculiar, showing narrow He and H lines in emission, indicative of interaction with circumstellar material (Pastorello et al. 2008b), and is considered a transitional object between SN 2006jc-like events, and SNe IIn. SN 2005la appears as a blue outlier in $B-V$, and it is bluer than the mean in $r'-i'$, evolving

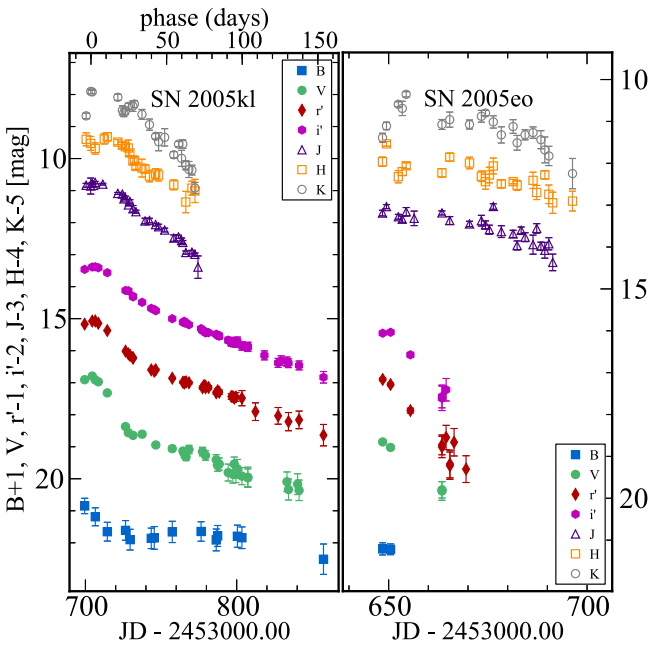

Figure 18. SN Ic SN 2005kl (left) and SN 2005eo (right), which was reclassified as a late SN Ia in M14. Both show uncharacteristically red colors. Note, however, the steeper slope of flux decay in SN 2005kl, consistent with a young SN evolution.

(A color version of this figure is available in the online journal.)

redward at late times (phase $\gtrsim$50 days). SN 2005la is also included in the D11 sample. We note that SN 2006jc and SN 2005la, both SNe interacting with a He-rich, and for SN 2005la also a H-rich, circumstellar medium have bluer $B-V$ colors than the rest of the normal stripped SNe. Figure 3 in Pastorello et al. (2008b) shows the $B-V$ evolution of SNe Ib-n (also including SN 2000er and SN 2002ao): all of these SNe have very blue colors ($-0.4 \lesssim B-V \lesssim 0.6$ mag for 0–100 days after maximum) when compared to non-interacting stripped SNe, as in our Figure 13. The bluer colors of these SNe Ib-n and SN 2005la are due to both a bluer continuum (most likely due to blending of Fe II lines from fluorescence; Foley et al. 2007) and strong He lines in emission.

7.3.4. SN 2005kl

SN 2005kl (light blue in Figure 13) is consistently and significantly redder than the sample mean throughout its color evolution in each color space. However, it is not spectroscopically peculiar.

The SN is in a bright and high-gradient galaxy, making image subtraction difficult and resulting in large error bars, especially in B. From the spectra published in M14, it is evident that the SN sits in an H II region. SN 2005kl is classified as a SN Ic in M14. The sparse spectral coverage cannot rule out the development of He I lines near peak, which would modify the classification to SN IIb. We note that SN 2005eo shows a qualitatively similar color evolution, with suppressed B flux and red colors. CfA light curves for both objects are shown in Figure 18. While SN 2005eo was initially classified as a SN Ic, and thus included in the D11 sample, we now reclassify it as a late SN Ia (M14).[22]

[22] The light curve was fitted with SNANA (Kessler et al. 2009), but with the little available data, the photometric fit remains inconclusive, although SN Ic provided worse fits than SN Ia's. Although SN 2005eo would not be a standard SN Ia, as its J-band flux fall is slow, the poor light curve fit to SN Ic templates reinforces our trust in the new spectroscopic classification.

With its reclassification, the earliest optical photometry in D11 is actually catching the second *R*-band peak of the late SN Ia. Both SN 2005kl and SN 2005eo are found in early-type spiral galaxies. Neither object suffers from significant galactic reddening (see Table 2). While SN 20005kl may show red colors similar to SN 2005eo, a SN Ia, we are certain that SN 2005kl is not a SN Ia since our CfA late-time, nebular spectra of SN 2005kl show strong emission lines of [O I] and [Ca II], characteristic of stripped SNe (M14).

8. CONCLUSIONS

This paper presents a densely sampled, homogeneous suite of photometric measurements of stripped SNe at optical and NIR wavelengths: U (before 2009 January) and u' (after 2009 January), BV, RI (before 2004 September) and $r'i'$ (after 2004 September), and JHK_s bands, including 61 objects covered in optical bands and 25 in NIR. These data were collected between 2001 and 2009 at FLWO.

Our photometry provides additional data for 37 supernovae already discussed in the literature and the first published measurements for 27 new supernovae. Among the objects previously published, we are publishing photometry for 6 objects studied in the literature at other wavelengths (radio or UV) or with methods different than photometry (e.g., spectroscopy or host and progenitor studies; see Table 1), but for which photometric measurements have not yet been published. Stripped SN spectroscopy from our group is presented in M14, complementing this data set with coverage for 54 of our total 64 objects.

This is the largest stripped SN data set to date, containing multi-color photometry in bands from optical U to NIR K_s. Our sample includes 64 stripped SNe, 22 with both optical and NIR measurements, 61 with optical measurements, and 25 with NIR measurements. This doubles the current supply of stripped SN objects in the literature. All SNe have multi-band data, allowing the determination of multiple colors. Our photometry (described in Sections 3.1 and 3.2) is produced from template-subtracted images, for all but six objects in optical bands and five in NIR, since those objects are well removed from their host galaxy. We compare our photometry with literature data (Section 5) and find agreement within the errors for most published SNe. However, we find D11 photometry to be brighter than ours by as much as one magnitude at peak and even more at late times. We attribute this discrepancy to host-galaxy contamination in the D11 data since the D11 photometric data are not based on template-subtracted images.

A solid determination of the epoch of maximum brightness in V band (JD_{Vmax}) is now possible for 37 objects using our data in combination with existing literature data (Section 4).

With these data, we investigated the color behavior of stripped SNe (Section 6), with the caveat that no corrections for host-galaxy extinction have been applied to our data. This approach captures the observed color behavior of stripped SNe (also adopted for SN rates in Li et al. 2011 for example), and simulates the parameter space of current and future optical and NIR surveys such as RATIR (Butler et al. 2012) and LSST (LSST Science Collaboration & LSST Project 2009), assuming that the reddening that the SNe in our sample experienced is representative.

We present an intriguing separation of different stripped SN subtypes in the $r'-i'$ versus $V-H$ color space, with SNe Ic-BL appearing bluer than both SNe Ib and Ic, based on the 19 stripped SNe for which JD_{Vmax} optical+NIR colors can be determined, but cautioning the reader that in our data set only two SNe Ic and two SNe Ic-BL have sufficient photometric coverage to be included in a $r'-i'$ versus $V-H$ color–color plot evaluated near peak (Figure 12). We also observe a very narrow distribution in $r'-i'$ color for SNe Ic-BL, with a standard deviation of only 0.01 mag around a mean $< r'-i' >_{\rm peak} = -0.025$ mag. This standard deviation is at least two times smaller than for any other subtype. As the data set grows, these color–color plots hold the promise of separating supernova types by photometry alone, especially with the advent of new NIR surveys (e.g., RATIR, Butler et al. 2012; Fox et al. 2012 and SASIR, Bloom et al. 2009).

In addition, we identify a number of individual SNe with peculiar color behavior, some of which were known to be peculiar from spectra (e.g., SN 2005la and SN 2006jc, both SNe whose ejecta are interacting with He-rich and for SN 2005la also H-rich circumstellar material), while others are spectroscopically normal (SN 2005kl).

Finally, spectra for over 80% of the objects we presented here are presented in a companion paper (M14). The availability of spectra with ample coverage at several epochs for most of our objects offers an opportunity for an accurate statistical assessment of the photometric diversity among stripped SNe types, which is necessary for classification in upcoming large synoptic surveys as well as for future progenitor studies.

We are immensely grateful for the efforts of the observers, particularly Perry Berlind, Michael L. Calkins, Gilbert A. Esquerdo, and Emilio E. Falco, who obtained the majority of the data presented here. In addition, we thank the staff of the F. L. Whipple Observatories for their extensive support and assistance.

The authors thank Saurabh Jha, Tom Matheson, Alex Filippenko, Ryan Foley, Nathan Smith, John Raymond, Rob Fesen, Chris Stubbs, Avishay Gal-Yam, Claes Fransson, Alicia Soderberg, and Eli Dwek for illuminating discussions. We thank Brandon Patel and Saurabh Jha for running SNANA fits.

F.B.B. is supported by a James Arthur fellowship at the Center for Cosmology and Particle Physics at NYU. M.M. is supported in part by NSF CAREER award AST-1352405. Supernova research at Harvard University has been supported in part by the National Science Foundation grant AST06-06772 and R.P.K. in part by the NSF grants AST09-07903 and AST12-11196, and in part by the Kavli Institute for Theoretical Physics NSF grant PHY99-07949. Observations reported here were obtained at the F.L. Whipple Observatory, which is operated by the Smithsonian Astrophysical Observatory (SAO). PAIRITEL is operated by the Smithsonian Astrophysical Observatory and was made possible by a grant from the Harvard University Milton Fund, the camera loan from the University of Virginia, and the continued support of the SAO and UC Berkeley. The data analysis in this paper has made use of the Hydra computer cluster run by the Computation Facility at the Harvard-Smithsonian Center for Astrophysics.

This research has made use of NASA's Astrophysics Data System Bibliographic Services (ADS), the HyperLEDA database, and the NASA/IPAC Extragalactic Database (NED) which is operated by the Jet Propulsion Laboratory, California Institute of Technology, under contract with the National Aeronautics and Space Administration. This publication makes use of data products from the Two Micron All Sky Survey, which is a joint project of the University of Massachusetts and the Infrared Processing and Analysis Center/California Institute of Technology, funded by NASA and NSF.

REFERENCES

Alard, C. 2000, A&AS, 144, 363
Alard, C., & Lupton, R. H. 1998, ApJ, 503, 325
Aldering, G., Adam, G., Antilogus, P., et al. 2002, Proc. SPIE, 4836, 61
Arkharov, A., Efimova, N., Leoni, R., et al. 2006, ATel, 961, 1
Bertin, E., Mellier, Y., Radovich, M., et al. 2002, in ASP Conf. Ser. 281, Astronomical Data Analysis Software and Systems XI, ed. D. A. Bohlender, D. Durand, & T. H. Handley (San Francisco, CA: ASP), 228
Bloom, J. S., Caldwell, N., Pahre, M., & Falco, E. E. 2003, Proposal, 1
Bloom, J. S., Prochaska, J. X., Lee, W., et al. 2009, arXiv:0905.1965
Bloom, J. S., Starr, D. L., Blake, C. H., Skrutskie, M. F., & Falco, E. E. 2006, in ASP Conf. Ser. 351, Astronomical Data Analysis Software and Systems XV, ed. C. Gabriel, C. Arviset, D. Ponz, & S. Enrique (San Francisco, CA: ASP), 751
Boisseau, J. R., & Wheeler, J. C. 1991, AJ, 101, 1281
Burbidge, E., Burbidge, G., Fowler, W., & Hoyle, F. 1957, RvMP, 29, 547
Butler, N., Klein, C., Fox, O., et al. 2012, Proc. SPIE, 8446, 844610
Cano, Z. 2013, MNRAS, 434, 1098
Clocchiatti, A., Wheeler, J. C., Phillips, M. M., et al. 1997, ApJ, 482, 675
Cutri, R. M., Skrutskie, M. F., van Dyk, S., et al. 2003, The IRSA 2MASS All-Sky Point Source Catalog, 2MASS All Sky Catalog of point sources (NASA/IPAC Infrared Science Archive; http://irsa.ipac.caltech.edu/applications/Gator/)
Drout, M. R., Soderberg, A. M., Gal-Yam, A., et al. 2011, ApJ, 741, 97
Drout, M. R., Soderberg, A. M., Mazzali, P. A., et al. 2013, ApJ, 774, 58
Elmhamdi, A., Danziger, I. J., Branch, D., et al. 2006, A&A, 450, 305
Filippenko, A. V. 1997, ARA&A, 35, 309
Filippenko, A. V., Barth, A. J., & Matheson, T. 1995, ApJL, 450, L11
Filippenko, A. V., Li, W. D., Treffers, R. R., & Modjaz, M. 2001, in IAU Colloq. 183, Small Telescope Astronomy on Global Scales, Vol. 246, ed. B. Paczynski, W.-P. Chen, & C. Lemme (San Francisco, CA: ASP), 121
Filippenko, A. V., Matheson, T., & Ho, L. C. 1993, ApJL, 415, L103
Fitzpatrick, E. L. 1999, PASP, 111, 63
Folatelli, G., Contreras, C., Phillips, M. M., et al. 2006, ApJ, 641, 1039
Foley, R. J., Smith, N., Ganeshalingam, M., et al. 2007, ApJL, 657, L105
Fox, O. D., Kutyrev, A. S., Rapchun, D. A., & Klein, C. R. 2012, Proc. SPIE, 8453, 845310
Friedman, A. S. 2012, PhD thesis, Harvard Univ.
Fukugita, M., Nakamura, O., Okamura, S., et al. 2007, AJ, 134, 579
Galama, T. J., Vreeswijk, P. M., van Paradijs, J., et al. 1998, Natur, 395, 670
Gallagher, J. S., Garnavich, P. M., Berlind, P., et al. 2005, ApJ, 634, 210
Gehrels, N., Chincarini, G., Giommi, P., et al. 2004, ApJ, 611, 1005
Hamuy, M., Pignata, G., Maza, J., et al. 2012, MmSAI, 83, 388
Hicken, M., Challis, P., Jha, S., et al. 2009, ApJ, 700, 331
Hicken, M., Challis, P., Kirshner, R. P., et al. 2012, ApJS, 200, 12
Hjorth, J., & Bloom, J. S. 2012, in The Gamma-Ray Burst–Supernova Connection, ed. C. Kouveliotou, R. A. M. J. Wijers, & S. Woosley (Cambridge Astrophysics Series 51; Cambridge: Cambridge Univ. Press), 169
Hjorth, J., Sollerman, J., Møller, P., et al. 2003, Natur, 423, 847
Jha, S., Kirshner, R. P., Challis, P., & Garnavich, P. M. 2006, AJ, 131, 527
Jha, S., Riess, A. G., & Kirshner, R. P. 2007, ApJ, 659, 122
Kasliwal, M. M., Kulkarni, S. R., Gal-Yam, A., et al. 2011, ApJ, 755, 161
Kessler, R., Bernstein, J. P., Cinabro, D., et al. 2009, PASP, 121, 1028
Kocevski, D., Modjaz, M., Bloom, J. S., et al. 2007, ApJ, 663, 1180
Landolt, A. U. 1992, AJ, 104, 340
Leloudas, G., Gallazzi, A., & Sollerman, J. 2011, A&A, 530, A95
Li, W., Filippenko, A. V., Treffers, R. R., et al. 2001, ApJ, 546, 734
Li, W., Leaman, J., Chornock, R., et al. 2011, MNRAS, 412, 1441
LSST Science Collaboration, & LSST Project. 2009, LSST Science Book (arXiv:0912.0201, http://www.lsst.org/lsst/scibook)
Maeda, K., Tanaka, M., Nomoto, K., et al. 2007, ApJ, 666, 1069
Malesani, D., Fynbo, J. P. U., Hjorth, J., et al. 2009, ApJL, 692, L84
Mannucci, F., Della Valle, M., Panagia, N., et al. 2005, A&A, 433, 807
Marion, G. H., Vinko, J., Kirshner, R. P., et al. 2014, ApJ, 781, 69
Mattila, S., Meikle, W. P. S., & Lundqvist, P. 2008, MNRAS, 389, 141
Maund, J. R., Wheeler, J. C., Patat, F., et al. 2007, MNRAS, 381, 201
Mazzali, P. A., Valenti, S., Della Valle, M., et al. 2008, Sci, 321, 1185
Miknaitis, G., Pignata, G., Rest, A., et al. 2007, ApJ, 666, 674
Modjaz, M. 2007, PhD thesis, Harvard Univ.
Modjaz, M. 2011, AN, 332, 434
Modjaz, M., Blondin, S., & Kirshner, R. P. 2014, AJ, 147, 99
Modjaz, M., Li, W., Butler, N., et al. 2009, ApJ, 702, 226
Modjaz, M., Stanek, K. Z., Garnavich, P. M., et al. 2006, ApJL, 645, L21
Nomoto, K., Iwamoto, K., & Suzuki, T. 1995, PhR, 256, 173
Nomoto, K., Tominaga, N., Umeda, H., Kobayashi, C., & Maeda, K. 2006, NuPhA, 777, 424
Pastorello, A., Mattila, S., Zampieri, L., & Della Valle, M. 2008a, MNRAS, 389, 113
Pastorello, A., Quimby, R. M., & Smartt, S. J. 2008b, MNRAS, 389, 131
Pastorello, A., Smartt, S. J., Mattila, S., & Eldridge, J. J. 2007, Natur, 447, 829
Patat, F., Cappellaro, E., Danziger, J., et al. 2001, ApJ, 555, 900
Paturel, G., Garcia, A. M., Fouque, P., & Buta, R. 1991, A&A, 243, 319
Paturel, G., Theureau, G., Bottinelli, L., et al. 2003, A&A, 412, 57
Pian, E., Mazzali, P. A., Masetti, N., et al. 2006, Natur, 442, 1011
Podsiadlowski, P., Langer, N., Poelarends, A. J. T., et al. 2004, ApJ, 612, 1044
Pritchard, G. H., Roming, P. W. A., Brown, P. J., Bayless, A. J., & Frey, L. H. 2013, ApJ, 787, 157
Quimby, R. 2006, PhD thesis, Univ. Texas at Austin
Rest, A., Stubbs, C., Becker, A. C., et al. 2005, ApJ, 634, 1103
Richardson, D., Branch, D., & Baron, E. 2006, AJ, 131, 2233
Richmond, M. W., Treffers, R. R., Filippenko, A. V., & Paik, Y. 1996, AJ, 112, 732
Riess, A. G., Kirshner, R. P., Schmidt, B. P., et al. 1999, AJ, 117, 707
Sahu, D. K., Tanaka, M., Anupama, G. C., Gurugubelli, U. K., & Nomoto, K. 2009, ApJ, 697, 676
Sako, M., Bassett, B., Becker, A. C., et al. 2014, arXiv:1401.3317
Sanders, N. E., Soderberg, A. M., & Valenti, S. 2012, ApJ, 756, 184
Sauer, D. N., Mazzali, P. A., Deng, J., et al. 2006, MNRAS, 369, 1939
Schechter, P. L., Mateo, M., & Saha, A. 1993, PASP, 105, 1342
Schlafly, E. F., & Finkbeiner, D. P. 2011, ApJ, 737, 103
Schlegel, D. J., Finkbeiner, D. P., & Davis, M. 1998, ApJ, 500, 525
Scolnic, D., Rest, A., Riess, A., & Huber, M. E. 2013, arXiv:1310.3824
Skrutskie, M. F., Cutri, R. M., Stiening, R., et al. 2006, AJ, 131, 1163
Smith, J. A., Tucker, D. L., Kent, S., et al. 2002, AJ, 123, 2121
Smith, N., Foloey, R. J., & Filippenko, A. V. 2008, ApJ, 680, 568
Soderberg, A. M., Berger, E., Page, K. L., et al. 2008, Natur, 453, 469
Stanek, K. Z., Matheson, T., Garnavich, P. M., et al. 2003, ApJL, 591, L17
Taubenberger, S., Pastorello, A., & Mazzali, P. A. 2006, MNRAS, 371, 1459
Tominaga, N., Tanaka, M., Nomoto, K., et al. 2005, ApJL, 633, L97
Uomoto, A., & Kirshner, R. P. 1986, ApJ, 308, 685
Valenti, S., Benetti, S., Cappellaro, E., et al. 2008, MNRAS, 383, 1485
Valenti, S., Fraser, M., Benetti, S., et al. 2011, MNRAS, 416, 3138
Wood-Vasey, W. M., Friedman, A. S., Bloom, J. S., et al. 2008, ApJ, 689, 377
Woosley, S. E., & Bloom, J. S. 2006, ARA&A, 44, 507
Woosley, S. E., Langer, N., & Weaver, T. A. 1993, ApJ, 411, 823